catalysts

MDPI

Article

Effect of the Addition of Alkaline Earth and Lanthanide Metals for the Modification of the Alumina Support in Ni and Ru Catalysts in CO_2 Methanation

David Méndez-Mateos, V. Laura Barrio *, Jesús M. Requies and José F. Cambra

School of Engineering (UPV/EHU), Plaza Ingeniero Torres Quevedo 1, 48013 Bilbao, Spain; david.mendez@ehu.eus (D.M.-M.); jesus.requies@ehu.es (J.M.R.); jose.cambra@ehu.es (J.F.C.)
* Correspondence: laura.barrio@ehu.eus

Abstract: In order to reduce greenhouse gas emissions, which are reaching alarming levels in the atmosphere, capture, recovery, and transformation of carbon dioxide emitted to methane is considered a potentially profitable process. This transformation, known as methanation, is a catalytic reaction that mainly uses catalysts based on noble metals such as Ru and, although with less efficiency, on transition metals such as Ni. In order to improve the efficiency of these conventional catalysts, the effect of adding alkaline earth metals (Ba, Ca, or Mg at 10 wt%) and lanthanides (La or Ce at 14 wt%) to nickel (13 wt%), ruthenium (1 wt%), or both-based catalysts has been studied at temperatures between 498 and 773 K and 10 bar pressure. The deactivation resistance in presence of H_2S was also monitored. The incorporation of La into the catalyst produces interactions between active metal Ni, Ru, or Ru-Ni and the alumina support, as determined by the characterization. This fact results in an improvement in the catalytic activity of the $13Ni/Al_2O_3$ catalyst, which achieves a methane yield of 82% at 680 K for $13Ni/14La\text{-}Al_2O_3$, in addition to an increase in H_2S deactivation resistance. Furthermore, 89% was achieved for $1Ru\text{-}13Ni/14La\text{-}Al_2O_3$ at 651 K, but it showed to be more vulnerable to H_2S presence.

Keywords: methanation; Ni catalysts; alumina; alkaline earth metals; lanthanides

Citation: Méndez-Mateos, D.; Barrio, V.L.; Requies, J.M.; Cambra, J.F. Effect of the Addition of Alkaline Earth and Lanthanide Metals for the Modification of the Alumina Support in Ni and Ru Catalysts in CO_2 Methanation. *Catalysts* **2021**, *11*, 353. https://doi.org/10.3390/catal11030353

Academic Editor: Patrick Da Costa

Received: 9 February 2021
Accepted: 2 March 2021
Published: 9 March 2021

1. Introduction

Greenhouse gases (GHGs) constitute part of the Earth's atmosphere naturally, maintaining the optimal conditions for life [1]. The ability of GHG to conserve part of the energy from solar radiation allows the planet's temperature to be moderate (17 °C global average) [2]. However, with the advent of the industrial revolution, new energy sources based on the combustion of fossil fuels appeared. With the increasing industrialization of the last century and a half, energy demand has been going up to gratify the growing food demand caused by the increase in the world's population. Moreover, large-scale agriculture has increased, this entails great deforestation to enlarge arable land. All this has meant that GHGs levels have reached levels never seen before. Carbon dioxide (CO_2) is especially important in composing two thirds of GHGs and whose emission is related to three quarters of the combustion of fossil fuels [3].

In the recent climatic summit of the United Nations of 2019, member countries were instigated to mobilize the implementation of several of the sustainable development goals for 2030, complying with the measures established by the 2015 Paris agreement. The objectives set include the reduction of greenhouse gas emissions up to 45% in 2030 and eliminating them in 2050 to limit the global warming to below 2 °C [4]. The strategies established by the European Union (EU) to achieve the agreed objectives consist of betting on energy efficiency, renewable energy, reducing emissions in transport and industry, and carbon capture and storage [5]. There are several possible ways to achieve the objectives in reducing GHGs emissions. The first way is the minimization of emissions by the capture

and storage of gases, a greater use of waste materials, an improvement of the efficiency of combustion systems, the implementation of more biomass-based energy systems, replacing traditional fuels with biofuels, or the proper management of arable land and cultivation techniques. However, at present it is strongly believed that the best way to achieve these objectives is the capture, transformation, and recovery of emitted gases, especially carbon dioxide. These gases would become other compounds that can be used to obtain fuels (methane, ethane), plastics (ethylene), medicines (formaldehyde), solvents (methanol, ethanol), or other uses (carbon monoxide, formic acid) [6]. The methanation of CO_2, studied by Sabatier (Equation (1) [7]), proposes a sustainable way to transform residual CO_2 into synthetic methane.

$$CO_2 + 4H_2 \rightleftarrows 2H_2O + CH_4 \qquad \Delta G = -114\ \text{kJ}\cdot\text{mol}^{-1} \tag{1}$$

This reaction constitutes the second stage of a larger process known as power-to-gas [8]. In this process, hydrogen is obtained from water electrolysis (Equation (2)) using energy from renewable sources, whose intermittent production would cause problems in the operability of the electricity grid [9].

$$H_2O \rightarrow H_2 + \frac{1}{2}O_2 \qquad \Delta G = 237.1\ \text{kJ}\cdot\text{mol}^{-1} \tag{2}$$

Obtaining methane by the Sabatier reaction is a favorable process from a thermodynamic point of view, but with kinetic limitations for the complete reduction of CO_2 to methane, due to its exothermic nature [10]. For this reason, various catalysts have been studied in order to overcome these limitations for methane production. Some of the metals that have proven to be active in methane production are noble metals such as ruthenium (Ru), rhodium (Rh), and palladium (Pd), but also nickel (Ni), and their combinations [10–24]. The most commonly used supports in the literature for the dispersion of these metals are metal oxides such as Al_2O_3, SiO_2, TiO_2, CeO_2, zeolites (among others) and even, in recent works, reduced graphene oxide (rGO) [12–22]. Nickel-based catalysts are common in the literature due to their competitive activity and low price, being proposed as a viable alternative to noble metals [10,13,17–19,21,23]. However, in order to verify the effect that the noble metal has on Ni, Mihet M. and Lazar M.D. [23] studied the addition of small amounts (0.5 wt%) of Pd, platinum (Pt), and Rh on Ni (10 wt%) catalysts in the methanation reaction. They demonstrated that doping Ni with Pd or Pt improves activity at lower temperatures, contrary to what happens when Rh is added. Renda et al. [25] studied the effect of incorporating different amounts of platinum and ruthenium (0.5, 1, and 3 wt%) on a catalyst based on ceria as support and the compared with nickel (10 wt%) as promoter. It was observed that the most suitable amount of ruthenium that improves the activity of the nickel catalyst is 1 wt%, the best value being 0.5 wt% in the case of platinum, reaching a high conversion at a lower temperature. A similar conclusion was found by Bustinza et al. [26], by incorporating ruthenium in different proportions and order on a nickel (12.7 wt%) catalyst supported in alumina-coated monolith. In this case, the best conversion in the methanation reaction was achieved for catalysts with 1 wt% of Ru.

Alumina is the most common catalyst support, due to its high surface area which favors the dispersion of the metal atoms, facilitating the access of reaction gases to the active center [13–15,19–23]. Namely, γ-Al_2O_3 structure favors metallic catalyst stability, activity and selectivity within the operation temperature range for this reaction, pointing to this support as one of the most suitable [27]. It has been shown in recent works that alumina support modification in Ni catalysts for the methane reaction increases activity, especially at low temperatures [19,28,29]. Liang et al. described an increment in the conversion of CO_2 at low temperatures after the addition of magnesium (Mg), calcium (Ca), strontium (Sr), and barium (Ba) to the Ni/alumina catalysts, especially the last two [28]. In the work of Tsiotsias et al. (2020) [30], it was shown that the incorporation of alkaline and alkaline earth metals increases the alkalinity of the support, facilitates the chemisorption of CO_2, increases the population of oxygen vacancies on the surface of the

metal oxide, and improves the dispersion of the metal on the support. Jomjaree et al. [31] prepared Ni/CeO_2 nanostructured catalysts with tunable CeO_2 morphology/structure determining the influence in increasing oxygen vacancies and oxygen storage capacity, and their influence on catalytic activity enhancement between 473 and 773 K under atmospheric pressure. Cardenas-Arenas et al. [29] prepared a 3D-ordered macroporous structure of NiO-CeO_2 mixed oxide (NiO-CeO_2 (np)) to achieve high CO_2 methanation conversion due to its high specific surface area if compared with a reference catalyst without size control (NiO-CeO_2 (Ref)). In addition, García-García et al. [19] studied the addition of cerium (Ce) to modified alumina loading 4 and 6 wt% of Ce and 3 wt% zirconium (Zr) increasing the yield to methane at low temperature [19]. However, there were small amounts of Ce and Zr and it was observed that at least a 6 wt% of Ce is needed to improve the catalyst activity towards methanation. Moreover, Ni-Ce-Zr catalyst increasing surface oxygen species implies the formation of intermediates enhancing the CO_2 conversion even at very low temperatures (473 K) [32]. Furthermore, the effect of modifying alumina support with different amounts of La (0, 4, 14, and 37 wt%) has also been studied by Garbarino et al. [29]. They concluded that the methane yield increases at low temperatures, as the La amount added increases to a maximum of 14 wt%. Finally, the modification of alumina supports with alkaline earth metals or lanthanides has been studied in other reactions (Fischer–Tropsch or dry reforming), showing an improvement in reaction performance [33–36].

In the present work, according to the previous observations of recent works, the effect of modifying the support of the 13Ni/γ-Al_2O_3 catalyst was studied. To that end, alkaline earth metals (Ba, Ca, and Mg) and lanthanides (La and Ce) were added to the bare support and their effect in catalyst containing Ru, Ni, and Ni-Ru as active metal on the CO_2 methanation reaction was examined. The Ni content used as promoter was 13 wt%, and that of Ru 1 wt%, based on previous studies already done by the research group, i.e., [37]. In the case of Ba, Ca, and Mg, it was 10 wt%, and in that of La and Ce, 14 wt%, justified by the above studies available in the bibliography.

2. Materials and Methods

2.1. Catalyst Preparation

The modified catalysts were prepared by wet impregnation methods in two successive stages. Determined amounts of γ-Al_2O_3 (Merck) and support modifying metals (barium nitrate 99.999% Sigma-Aldrich, calcium nitrate tetrahydrate 99% Sigma-Aldrich, magnesium nitrate hexahydrate 99% Sigma-Aldrich, lanthanum (III) nitrate hydrate 99.9% Sigma-Aldrich, and Cerium (III) nitrate hexahydrate 99.999% Sigma-Aldrich), were mixed in appropriate proportions (10 wt% Ba, Ca, or Mg; or 14 wt% La or Ce). Twenty milliliters of distilled water were added to the mixed salt supports and the pH value of γ-Al_2O_3 (7.5) was fitted over point of zero charge (pzc) at 8.5 [27,38]. The pH was adjusted adding ammonium (Panreac) to increase or nitric acid (Scharlau) to decrease the pH value. The solution was stirred overnight, in a rotary evaporator (Heidolph Laborota 4000) and the solvent was evaporated, heating at 338 K, and reducing slowly the pressure until 40–100 mbar helped by a vacuum pump. The support obtained was dried in an oven at 373 K during 2 h and calcined at 673 K in presence of air for 2 h, with a ramp of 1 K/min.

The catalysts were prepared by adding the metal salt of nickel (II) nitrate hexahydrate 99.999% (Sigma Aldrich) and/or ruthenium (III) chloride hydrate 99.98% (Sigma-Aldrich) to the prepared support and mixing with 20 mL of distilled water to obtain catalysts with 13 wt% of nickel, 1 wt% Ru, or both. The procedure was like the support preparation, using the wet impregnation method: pH control at 8.5, overnight stirring, solvent evaporation, drying, and calcining.

Finally, the calcined catalysts were pressed and sieved to the desired particle size: 0.42 mm < d_p < 0.50 mm. This particle size (d_p) was chosen in order to avoid reagents bypassing near the wall, by keeping an internal pipe diameter-to-particle size ratio higher than 10 [39].

The catalysts prepared were named, according to their nominal composition, as follows: 13Ni/10Ba-Al_2O_3, 13Ni/10Ca-Al_2O_3, 13Ni/10Mg-Al_2O_3, 13Ni/14Ce-Al_2O_3, 13Ni/14 La-Al_2O_3, 1Ru/14La-Al_2O_3, 1Ru-13Ni/14La-Al_2O_3, 1Ru-13Ni/Al_2O_3, and 1Ru/Al_2O_3.

2.2. Catalyst Characterization

The N_2 adsorption-desorption method was employed to evaluate the textural properties of the catalysts in the Autosorb 1C-TCD, after outgassing the samples at 573 K for 3 h. The specific surface area was calculated using Brunauer–Emmett–Teller (BET) equation and pore volume and pore sizes were calculated by the Barrett–Joyner–Halenda (BJH) method.

- The real composition of the catalysts was determined by inductively coupled plasma optical emission spectroscopy (ICP-OES) on a Perkin–Elmer Optima 3300DV. Moreover, after disaggregating the catalyst in acid solution (mixture of HCl 3:1 and HNO_3), the composition and chemical element were identified by characteristic wavelength emission intensity.
- The crystalline species and an approximation of the average crystal size (estimated by XRD patterns and Scherrer equation [40]) of the catalysts were carried out on a PANalytical X'Pert Pro diffractometer using a CuK_α radiation (λ = 0.15418 nm) at 40 kV and 30 mA and a scanning angle (2θ) of 20° to 90°.
- X-ray photoelectron spectroscopy (XPS) was obtained on a SPECS (Berlin, Germany) system equipped with a Phoibos 150 1D-DLD analyzer and an Al Kα (1486.6 eV) monochromatic radiation source with electrons output angle of 90°. XPS is a technique that allows the study of the species present on the surface of the catalyst and their chemical state.
- The temperature-programmed reduction of H_2 (H_2-TPR) and temperature programmed desorption of ammonia (NH_3-TPD) or of CO_2 (CO_2-TPD) were carried out in a Micromeritics AutoChem II RS232, equipped with a thermal conductivity detector (TCD). The TPR profiles were recorded heating 50 mg of the sample from 323 K to 973 K, at a ramp rate of 10 K/min. Previously, the sample was heated from room temperature to 473 K for 1 h in Ar stream (30 Nml/min). Later, the sample was cooled down to 323 K and the Ar was replaced by 5 vol.%, H_2/Ar (45 Nml/min) stream and analyzed. The TPD profiles were recorded after reducing the sample with 5 vol.%, H_2/Ar (45 Nml/min) stream, and heating to 723 K. Then, the sample was cooled with He, replacing this stream by 10 vol.% NH_3/He or CO_2 stream during 30 min. Recovering the He stream, NH_3 desorbed per unit time and catalyst mass was determined heating the sample from 423 K to 1173 K, at a ramp rate of 10 K/min.

2.3. Activity Test

The CO_2 methanation was carried out in a stainless steel fixed bed reactor of 32 cm of length, with an outside diameter of $\frac{1}{4}$", placed inside a bench-scale plant (PID Eng&Tech), at 10 bar and temperature range from 498 to 773 K. The reactor was loaded with 60 mg of catalyst, and diluted with inert SiC, in order to minimize thermal gradients in the catalytic bed ($weight_{catalyst}/weight_{SiC}$ = 1:4.5). Furnace temperature was adjusted to maintain the catalyst bed under isothermal condition using four thermocouples. The first step was the catalyst activation, reducing the catalyst with a mixture of N_2 (99.999%, Air Liquide) and H_2 (99.999%, Air Liquide) with a ratio of H_2/N_2 equal to 3:1 (65 Nml/min of H_2) at 673 K during 4 h. The reduction temperature of the catalysts was determined from the reduction profiles obtained by the TPR-H_2, finding 673 K as a suitable temperature for activating the catalysts. Even more, this temperature was the same for all of them so the results could be comparable. Once the catalyst was activated, the reaction gases, H_2 and CO_2 (99.98%, Air Liquide), were fed in a ratio H_2/CO_2 of 4:1 such that the weight hourly space velocity (WHSV) of the flow fed was 38.30, 60.80, or 128.75 $g_{feed}/(g_{cat} \cdot h)$, depending on the amount of catalyst used 200, 125, or 60 mg respectively.

The stoichiometry proportion for the methanation reaction was employed to obtain methane and water (Equation (3)). The methanation reaction is the combination of

Equations (4) and (5), where CO could be generated as an intermediate product, or as a final product in combination with methane [21].

$$CO_2 + 4\,H_2 \rightleftarrows CH_4 + 2\,H_2O \quad (3)$$

$$CO_2 + H_2 \rightleftarrows CO + H_2O \quad (4)$$

$$CO + 3\,H_2 \rightleftarrows CH_4 + H_2O \quad (5)$$

The reactor was heated at a rate of 10 K/min under N_2 flow, until the reaction temperature was reached. Afterwards, the N_2 flow was replaced by the mixture of reactants. The catalyst activity was studied at reaction temperatures from 498 K to 573 each 25 K and from 573 K to 773 K each 50 K. The products were separated in a Peltier condenser (condensed water and gas products), and then analyzed on-line using a Varian CP-4900 MicroGC equipped with a high sensitivity TCD and two columns (10 m Molecular Sieve 5, 10 m Poraplot Q). The reaction was stabilized at each temperature for 120 min, recording the output flow and composition of gases every 10 min. The water produced was collected and weighted in this time. The gas phase composition was on-line analyzed. The CH_4 yield was calculated using the following equation:

$$\eta_{CH_4} = \text{mol } CH_4^{out}/\text{mol } CH_4^{out}\text{stoichiometric}\cdot 100 \quad (6)$$

In the Equation (6), η_{CH_4} represents the methane yield, mol $CH_4{}^{out}$ represents the flow rate of the methane out of the reactor, and mol $CH_4{}^{out}$ stoichiometric represents the theorical flow rate of the methane out of the reactor, based on the stoichiometry of the Sabatier reaction. Thus, if all CO_2 is converted to CH_4, the value of η_{CH_4} would be 100%.

All the experiments were repeated to ensure reproducibility.

3. Results and Discussion

3.1. Catalyst Characterization

3.1.1. ICP Analysis

The chemical composition of the calcined catalysts employed in the CO_2 methanation was measured by ICP-OES analyses. The catalysts were prepared to have a target nominal content of 13 wt% for the Ni, 1 wt% for Ru, 10 wt% for the alkaline earth Ba, Ca, and Mg, and 14 wt% for the lanthanides La and Ce. Catalysts that only contain Ni showed a Ni content slightly higher than the target, as reported by García-García I. et al. [19] for a Ni catalyst supported on γ-Al_2O_3. However, the experimental nominal content of Ni was higher or lower than the target composition depending on the metal modifying the support. In the presence of La, the amount of Ni determined was greater than expected, as it was observed experimentally and confirmed in the literature [41,42]. In the case of Ca and Mg, a considerable decrease in its value was observed with respect to 13Ni/Al_2O_3. Moreover, a decrease in the proportion of Ni with respect to Ba was produced by the presence of Ba modifying the support. The catalyst, whose support was modified with Ce, slightly reduced the Ni content. In contrast, the catalyst 1Ru-13Ni/Al_2O_3 showed slightly higher nickel and lower Ru contents respective to the expected values. The chemical composition measured by ICP of the prepared catalysts and their target nominal contents (in brackets) are shown in the Table 1.

Table 1. Summary of the contents (wt%) of Ni, Ru, and modifier metal (M), textural properties, Ni crystal size.

Catalyst	Nominal Content			Measured Content by ICP			S_{BET} [a] (m^2/g)	V_P [b] (cm^3/g)	D_P [c] (nm)	S_{XRD} [d1] (nm)	S_{XRD} [d2] (nm)
	Ni	Ru	M	Ni	Ru	M					
γ-Al_2O_3	–	–	–	–	–	–	202	0.81	7.7	–	–
13Ni/Al_2O_3	13	–	–	13.9	–	–	180	0.55	7.2	5	10
13Ni/10Ba-Al_2O_3	13	–	10	8.83	–	14.17	93	0.12	6.9	5	15
13Ni/10Ca-Al_2O_3	13	–	10	15.73	–	7.27	74	0.08	6.1	10	25
13Ni/10Mg-Al_2O_3	13	–	10	17.52	–	5.48	109	0.15	7.3	5	15
13Ni/14Ce-Al_2O_3	13	–	14	12.16	–	14.84	86	0.12	7.2	5	15
13Ni/14La-Al_2O_3	13	–	14	15.41	–	11.59	79	0.11	6.5	5	15
1Ru/14La-Al_2O_3	–	1	14	–	1.19	13.81	129	0.17	7.2	–	–
1Ru-13Ni/14La-Al_2O_3	13	1	14	14.79	0.52	12.69	93	0.12	7.1	5	15
1Ru-13Ni/Al_2O_3	13	1	–	13.73	0.27	–	163	0.22	7.5	5	15

[a] The surface area was calculated by the Brunauer–Emmett–Teller (BET) method; [b] Barrett–Joyner–Halenda (BJH) desorption pore volume; [c] BJH desorption average pore diameter; [d] S_{XRD} [d1] (after reduction) and S_{XRD} [d2] (after reaction) represent Ni crystallite size approximation calculated from Ni (111) plane using Scherrer equation.

3.1.2. BET Measurements

In Table 1, the surface area, pore volume, and pore size are represented in order to analyze the textural properties of supports and prepared catalysts. The isotherms obtained for the supports and catalysts are IV-type curves, with a remarkable H_2 hysteresis loop, representative of mesoporous structure and due to the presence of "ink-bottle" or cylindrical channels [43].

The addition of Ru barely reduced the surface area of the alumina support (202 m^2/g), due to its small amount added. Contrary to what happened with the addition of Ni, a significant reduction of the surface area and pore volume were detected, probably due to the partial blockage of the small pores of the support [44]. The addition of a second metal contributed to the pore blocking effect depending on the metal and its interaction with the support. In the case of Mg, the surface area (and pore volume and size) reduction was lower than in the cases of Ca and Ba due to the creation of porous structures during the catalyst calcination stage [28]. The addition of Ba in amounts greater than 5 wt% produced the higher occupation by the metal, causing the reduction of the total surface area [28]. Ca promoted the coalescence of small pores to obtain larger pores during the calcination step, being increased with the amount of metal added [28]. The incorporation of La or Ce as support modifiers has an effect similar to that observed for alkaline earths, so that as metal was added to the catalyst, the sintering increased, producing a blockage of the small pores of the supports and the increase of pore size via merge of the catalysts.

3.1.3. H_2-TPR Studies

The effect of the alkaline earth and lanthanides on the reducibility and the metal-support interaction of the catalysts was evaluated using the H_2-TPR. Measurements and results are collected in the Figure (Figures 1 and 2). According to the reducibility and the strength of interaction Ni-support, the peaks represented in the H_2-TPR show four reducible species of nickel oxides. In the range of 523 to 623 K, reducible species correspond to nickel oxide with weak interaction with the support. The NiO with weak-medium interaction with the support corresponds to the reducible species between 623 K and 773 K. Stronger interaction (medium-strong) with the support for the Ni^{2+} occurs in the range of 773 to 1023 K for the non-stoichiometric nickel aluminate (NiO-Al_2O_3), the stoichiometric nickel aluminate species ($NiAl_2O_4$) being harder to reduce. These are reducible from 1073 K having a strong interaction with the support [28,45–48].

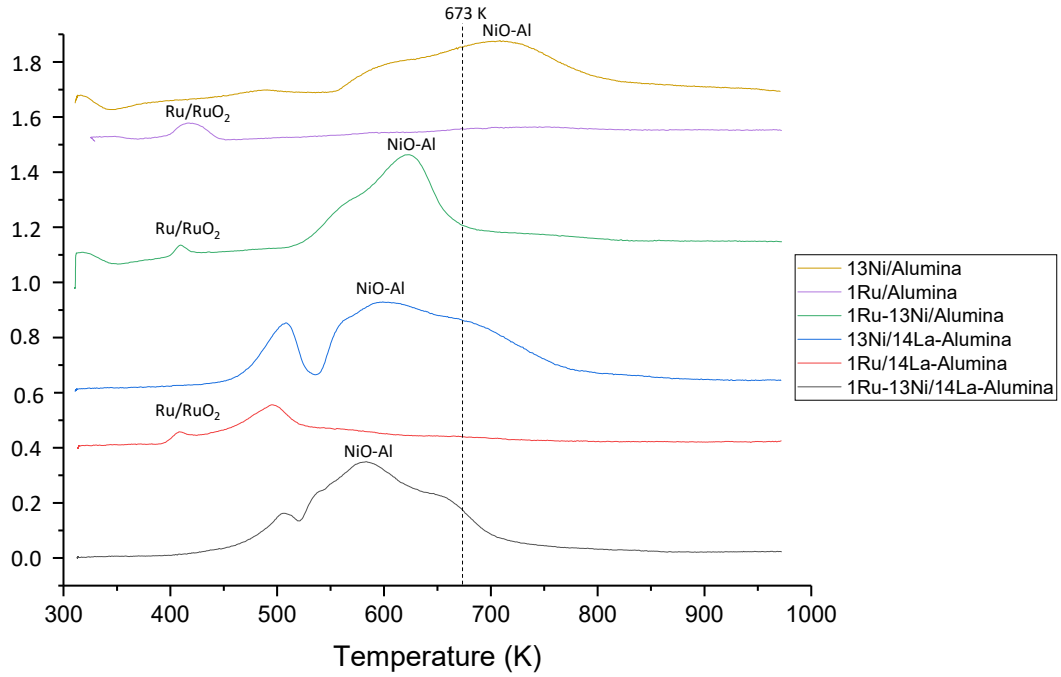

Figure 1. H_2-TPR (temperature-programmed reduction) profiles of the prepared catalysts of Ru, Ni, and La in 4% H_2/Ar atmosphere and 10 °C/min heating rate.

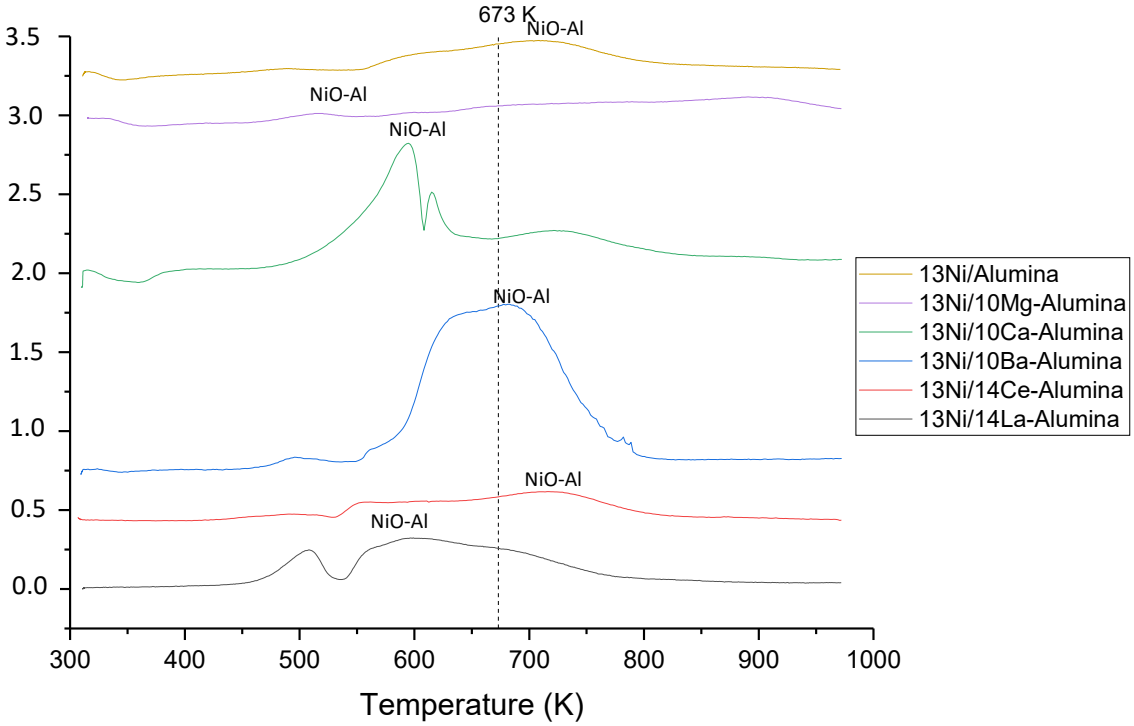

Figure 2. H_2-TPR profiles of the prepared catalysts of Ni, Ba, Ca, Mg, Ce and La in 4% H_2/Ar atmosphere and 10 °C/min heating rate.

The addition of noble metals, such as Ru, changes the reduction profiles of the Ni-catalyst as reported in the literature [19,49,50]. The reduction profile of the Ru catalyst showed a maximum located at 416 K corresponding to the reduction of supported RuO_2 into metallic Ru and a shoulder at 348 K according to the reduction of well-dispersed RuO_x species [50]. The catalyst of Ru and Ni exhibit mainly two peaks at 410 and 623 K and two

shoulders at 376 and 562 K, respectively. The peak and shoulder reported at 410 and 376 K correspond to those determined for the monometallic catalyst of Ru. The main reduction peak reported at 623 K represents NiO reduction, and the shoulder at 562 K represents the reduction of RuO_2 and NiO on the alumina surface, mainly forming Ni-Ru particles [49].

TPR patterns of La modified supports show a splitting of the peaks at temperatures between 500 and 700 K. The new peak at 505 K corresponds to free NiO species in the alumina support, which increases as the La content of the catalyst increases [29,45,51]. Based on the results and the literature observations, the stable La-alumina structure weakens the interaction between NiO and support as La content increases, by partial destruction of metastable Ni-Al mixed oxide phase [45,51].

As reported in literature, the addition of Ce to an alumina support results in hydrogen consumption due to different interaction of ceria with the support [52]. The reduction peaks were found at 598, 798, and 993 K corresponding to non-stoichiometric CeO_2, surface reducible metal centers of CeO_2, and bulk reducible centers of CeO_2, respectively [52]. Attending to the TPR profile obtained, the participation of the support in the reducibility of the nickel catalyst was observed at low reduction temperatures (561 K), corresponding the reduction peak at medium temperature (715 K) with the interaction of NiO with the support. At low temperature, the reduction peak represents the contribution in the reduction of Ni and Ce^{4+} at the surface of CeO_2 [52].

The TPR profiles of the supports of Ni catalysts modified with alkaline earth define a different spectrum, depending on the metal. Barium in contact with the alumina support produces reducible species as $BaAl_2O_4$ that at 763 K show a reduction peak. In combination with nickel, the greatest contribution in the TPR profile corresponds to the reduction of nickel species (with reduction peaks at 583, 903, and 1053 K), being facilitated the interaction of Ni and alumina by the presence of Ba. The contribution of Ba was mainly observed in the increase of the first two catalyst reduction peaks and decrease in the third, due to the interaction of BaO with the support, forming other structures (as spinel) [53]. The experimental profile presented three peaks and one shoulder at 498, 650, 682, and 561 K, respectively, as the literature shows [28,53]. The contribution of Ca is due to the presence of CaO in the catalyst, which is related to reduction at low temperatures, strengthening the interaction with NiO and improving the reducibility of Ni [28]. This produces a splitting of the low temperature reduction peak corresponding with the reduction of NiO, obtaining two peaks at 595 and 615 K. The first one increases with respect to the second, as the amount of Ca added increases [54]. It was observed that the addition of Mg (presented in form of MgO) decreased the reduction peaks corresponding to NiO and Ni aluminate [55]. In the TPR profile obtained for Ni/Mg-Alumina, three peaks at 513, 600, and 890 K were determined, with lower hydrogen consumption regarding to other catalysts analyzed. Some causes attributed by Tan et al. [55] are the effect of coverage of MgO on the NiO species; a strong interaction between NiO and MgO; a formation of larger Ni(Mg)O; or the combination of some of them [28]. NiO-MgO catalysts usually form NiO-MgO solid solution, which makes it very difficult to reduce, thus, it is reduced at higher temperatures. Its reduction usually gives very well dispersed crystals, as observed in the Requies work [56]. In general, according to the above, the addition of Ba facilitates the reduction of the catalyst against the use of Ca and Mg that makes it more difficult.

Based on the results obtained and the literature, the catalysts activated by the reduction at 673 K should be completely reduced at the reaction conditions between 498 and 773 K.

3.1.4. NH_3 and CO_2-TPD Studies

The acidity and basicity of the catalysts was studied by NH_3-TPD and CO_2-TPD desorption profiles, determining the quantity and strength of catalyst acid and basic sites, respectively. Desorption temperature determines the strength of the bonds, so that higher desorption temperature means stronger bond.

According to their nature, acid centers of different strength and adsorbed NH_3 reaction towards NO_x formation, define three regions: up to 523 K, weak acid sites (Lewis nature);

from 523 to 673 K, middle acid sites (Lewis); and strong acid sites (Brönsted nature) from 673 K [41,49,57]. Depending on the metal modifying the alumina support of the catalyst and according to the metal active phase, the NH_3-TPD profiles will be different. These profiles are shown in Figures 3 and 4. The main peaks are shown at around 520 and 541 K corresponding to Lewis acid sites (middle acidity) and 599 K, 825 K, and 1093 K conforming to Brönsted acid sites (strong acidity). The total amount of acid centers, and their distribution, related to ammonia desorption, are presented in Table 2 for the studied range, calculated as the area under the concentration-time curve of the TPD profiles, according to regions. The Lewis acid sites of alumina are coordinated with NH_3, due to the electron deficiency of trivalent aluminum atoms, presenting a maximum centered at 548 K [57]. Furthermore, the peak centered at 1073 K (strong acid region) was the most significant in the catalysts studied and corresponds with Brönsted acid sites where the hydrogen atoms may act as proton donor [58].

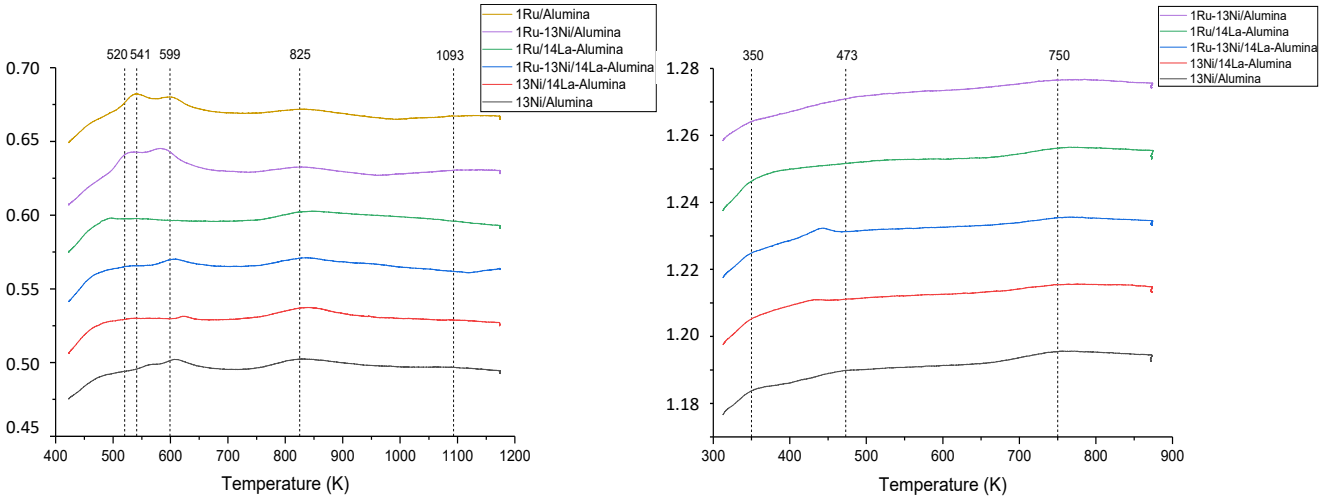

Figure 3. NH_3-TPD (temperature-programmed desorption) and CO_2-TPD profiles of the prepared catalysts of Ru, Ni, and La.

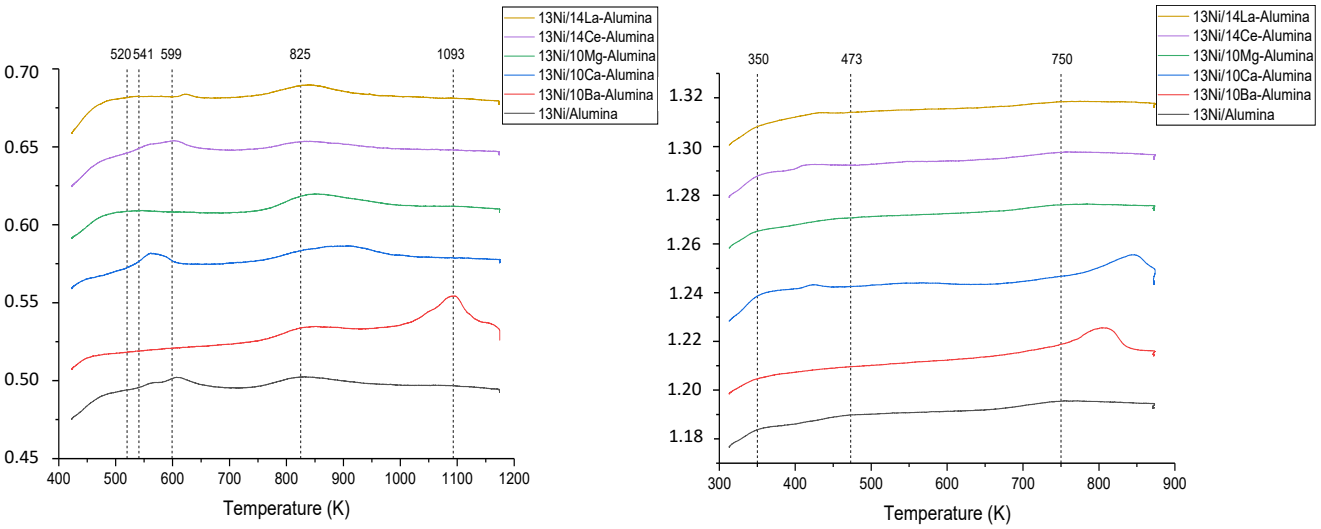

Figure 4. NH_3-TPD and CO_2-TPD profiles of the prepared catalysts of Ni, Ba, Ca, Mg, Ce, and La.

Table 2. Distribution of the strength of acidity and basicity by NH_3-TPD and CO_2-TPD, respectively, of the different catalysts.

Catalyst	Acidity Amount μmol NH_3/g_{cat}			Basicity Amount μmol CO_2/g_{cat}		
	Weak	Media	Strong	Weak	Media	Strong
Temperature	**<523**	**523 < T < 673**	**>673**	**<423**	**423 < T < 723**	**>723**
$13Ni/Al_2O_3$	127.3	337.9	1146.2	11.0	56.7	100.8
$13Ni/10Ba\text{-}Al_2O_3$	85.7	197.3	1407.3	12.7	64.6	127.4
$13Ni/10Ca\text{-}Al_2O_3$	83.7	260.2	1091.1	18.1	70.6	124.5
$13Ni/10Mg\text{-}Al_2O_3$	119.6	251.2	1116.5	15.6	79.3	143.0
$13Ni/14Ce\text{-}Al_2O_3$	143.1	383.2	1274.8	14.2	62.0	105.2
$13Ni/14La\text{-}Al_2O_3$	166.8	345.3	1268.7	15.2	70.8	118.5
$1Ru\text{-}13Ni/14La\text{-}Al_2O_3$	167.4	378.8	1253.1	13.4	65.8	108.5
$1Ru/14La\text{-}Al_2O_3$	165.5	316.2	1180.7	10.8	64.9	112.3
$1Ru\text{-}13Ni/Al_2O_3$	169.1	470.7	1167.0	12.7	55.8	91.9
$1Ru/Al_2O_3$	153.6	411.3	974.6			

The $13Ni/Al_2O_3$ catalyst is characterized by having a small peak at 460 K in weak acid region; two peaks in the medium acid region, with a main peak at 599 K and a weaker peak at 552 K; and another two wider peaks in the strong acid region at 825 K and 1093 K. In the case of the $1Ru/Al_2O_3$ catalyst, the peaks present in the region of medium acidity are more significant, taking into account the profile of Figure 3. These peaks appear at 541 and 599 K. This catalyst shows a quantitatively greater number of weak and medium acid centers than $13Ni/Al_2O_3$ catalyst. However, the peak present in strong acid regions is significantly lower for ruthenium. Therefore, the combination of both metals, Ru and Ni, produces an additive effect on the number of weak and medium acid centers. Thus, a significant increase in these centers is observed with respect to the Ni catalyst (and that of Ru), exhibiting two peaks similar to those of Ru, slightly displaced at lower temperatures. These peaks appear at 520 K and at 485 K.

Ba produces a significant decrease in the number of weak and medium acid centers, compared to the sharp increase in strong acid centers, due to the presence of two peaks, one smaller at 825 K and the other more noticeable at 1093 K. It is observed in $13Ni/10Ca\text{-}Al_2O_3$ catalyst, that the presence of Ca produces a migration of the density of active centers towards a medium interaction strength, close to a low interaction, at 558 K and to the region of strong centers at 915 K. However, despite its concentration, the density of acid centers in this case decreased for all strengths. Something similar happens to $13Ni/Mg\text{-}Al_2O_3$ catalyst, concentrating the centers mainly in the region of strong acid centers with a wide peak at 845 K and with a significant reduction in the density of centers of medium strength. The Ce-incorporating catalyst shows little significant difference from $13Ni/Al_2O_3$ spectrum, except for a slight increase in the density of active centers in all regions.

Finally, the addition of La to the catalysts containing Ru, Ni, or both demonstrates its contribution to the significant increase in the density of acid centers of higher strength. This effect is justified in the literature, referring to an interaction that takes place between La^{3+}-O^{2-} pairs with the strongest acid and basic centers of alumina. This results in the reduction of Lewis acidity, as was more easily observed in $1Ru/Al_2O_3$ catalyst, but providing stronger acid-basic couples [41].

Figures 3 and 4 show the CO_2-TPD profiles defined by the catalysts studied. The curves defined in this analysis define the distribution of basic catalyst centers as a function of temperature. In this way, as temperature increases, interaction between CO_2 and catalyst is stronger and, therefore, the basic centers are stronger. According to the strength of the basic centers of the catalyst, three regions of the curve are distinguished: the region of weak basic centers (between 313 and 423 K), moderate basic centers (between 423 and 723 K), and strong basic centers (between 723 and 823 K). Total basicity in each region are shown in Table 2.

The incorporation of alkaline earth elements and lanthanides to the catalyst structure contributes to the increase of basic centers that facilitate the adsorption of CO_2 for its reaction with H_2. The low electronegativity of these metals results in the metal oxide formed having a basic behavior [59]. In this way, the presence of these metals increases the number of basic centers of 13Ni/Al_2O_3 catalyst, as observed in the table for the three regions, especially for 13Ni/10Mg-Al_2O_3 catalyst.

The CO_2-TPD profiles are similar in the catalysts analyzed, having in common the presence of three peaks that appear at temperatures of 350, 473, and 750 K. The first, in the region of weak centers, corresponds to the formation of carbonates on the catalyst surface. Second, the peak appearing in the moderate region, at 473 K, is due to bicarbonate formation on the catalyst surface. Finally, when the interaction between CO_2 and catalyst is stronger (750 K), the formation of monodentate bicarbonate species takes place [60]. In the 1Ru-13Ni/14La-Al_2O_3, 13Ni/14Ce-Al_2O_3, and 13Ni/10Ca-Al_2O_3 catalysts, the formation of bicarbonate species is facilitated at lower temperatures, with the corresponding peak appearing at a temperature of approximately 423 K. The incorporation of Ba and Ca to the 13Ni/Al_2O_3 catalyst produces an increase in strong basic centers (although without reaching the one that produces 13Ni/10Mg-Al_2O_3), shifting the peak corresponding to the formation of monodentate bicarbonate species to 808 and 846 K, respectively. The number of strong basic centers is also remarkable. This demonstrates the strong character of the interactions of these catalysts with CO_2, interacting with the monodentate species of the bicarbonate species. In ceria-supported catalysts, the presence of medium-strength basic sites significantly improved the catalytic activity, as demonstrated by Liu et al. [61]. Alumina is known for its acidic character, but the intermediate strength basic sites led to an increase in the CO_2 adsorption capacity enable.

3.1.5. XPS

The XPS technique allowed us to determine the species present on the surface of the catalyst, their oxidation state and their quantification. The main species identified on the surface correspond to the support, identifying Al 2p at 74.2 eV and O 1s at 531.0–531.8 eV that make up the alumina and the oxides of the rest of the metals. Nickel is the main active metal of the catalysts studied, showing a multiple split peak at 854–854.5, 855.7–857.2, and 860.8–862.6 eV [62] according to Ni^0, Ni^{2+} from $NiAl_2O_4$, and Ni^{2+} satellite respectively for fresh catalyst [62], as observed in Figures 5 and 6. Used catalyst (after activity test and H_2S exposure) also showed three peaks in 13Ni/14La-Al_2O_3 and 1Ru-13Ni/14La-Al_2O_3, at 855.1, 857.5 and 862.8 eV, corresponding to Ni^{2+} from NiO, Ni^{2+} from $NiAl_2O_4$, and Ni^{2+} satellite respectively, and only two in the others at 855.8–856.6 and 862.0–863.0 eV, corresponding to Ni^{2+} from $NiAl_2O_4$, and Ni^{2+} satellite, respectively, as observed in Figures 5 and 6. Specifically, in fresh catalysts, a greater intensity of the metallic nickel peak than of the oxide is observed, due to the in situ reduction stage in the reduction cell incorporated in the equipment. However, in the case of the used catalysts, without reducing treatment, and due to the aggressive effect of temperature, the effect of hydrogen sulfide poisoning and sintering, only the presence of nickel aluminate is determined in most catalysts, identifying nickel oxide only in catalysts composed of Ni-La. The disappearance of metallic nickel in its transformation into nickel oxide or nickel aluminate can cause loss of activity of the catalyst.

Ru 3p 3/2 at 459.5–461.9 eV, used as an active metal or mainly as a promoter, was difficult to identify in some of the catalysts due to its low concentration, which approximates its spectrum to that of noise. The rest of the metals incorporated in the support were also identified. Ba 3d 5/2 with doublet at 781.1–781.9 and 796.4–797.2 eV with overlap in the Auger Ba MNN line that can lead to an underestimation of %Ni. Ca 2p at 346.7–347.5 eV. Mg 2p at 49.5–49.6 eV. Ce with quintuplet 3d 5/2 and 3d 3/2 in positions 880.0–880.6 and 885.0–885.5 eV for Ce^{3+} duplicated at 898.3–898.9 and 903.5–904.1 eV. In addition, at 882.1–882.9, 888.1–889.0 and 897.2–898.2 eV for Ce^{4+} duplicated at 900.4–901.2, 906.9–907.6, and 915.8–916.5 eV. Thus, in the less energetic positions, there is a slight

inclusion of the Ce spectrum in that of Ni, which hinders the identification of nickel 2p $\frac{1}{2}$ and underestimate %Ni.

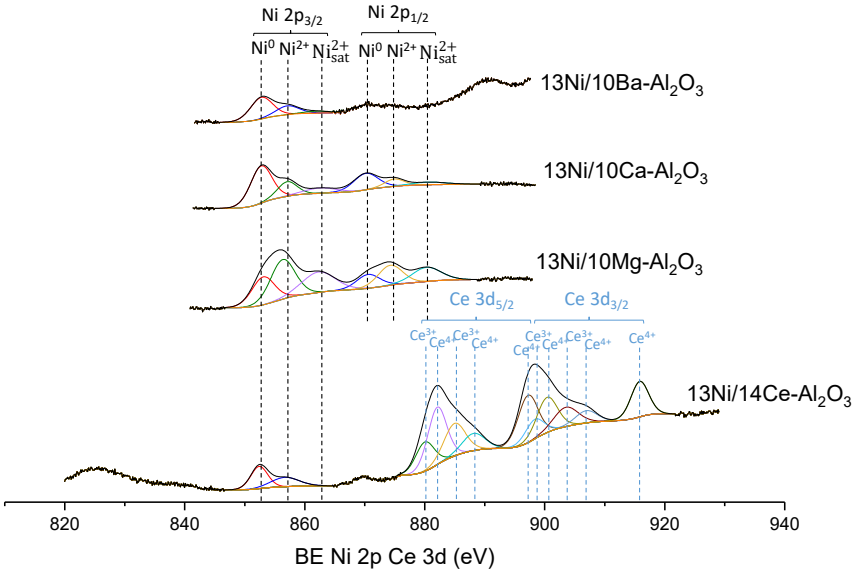

Figure 5. X-ray photoelectron spectroscopy (XPS) spectra of Ni $2p_{3/2}$, Ni $2p_{1/2}$, Ce $3d_{5/2}$, and Ce $3d_{3/2}$ regions of fresh catalysts.

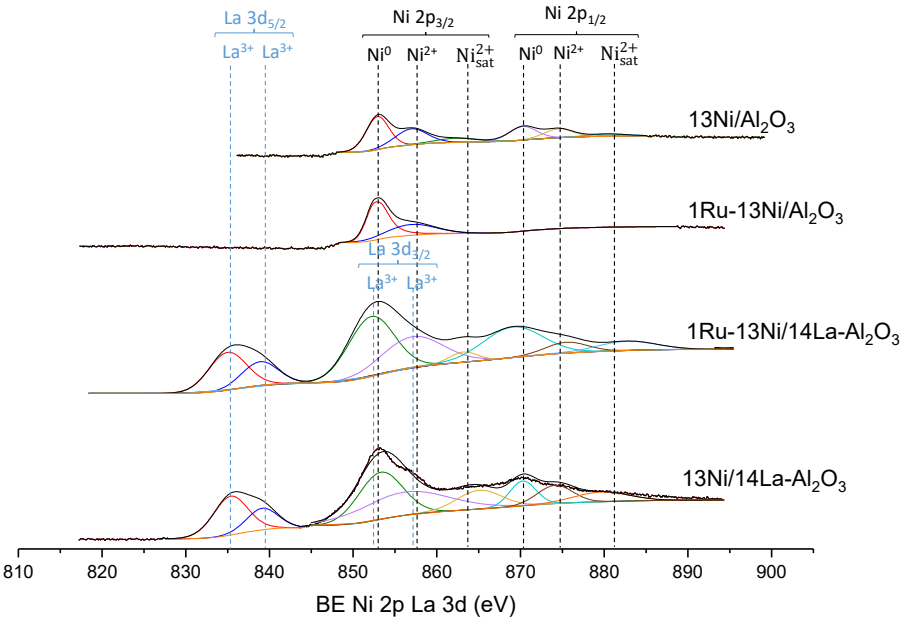

Figure 6. XPS spectra of La $3d_{5/2}$, La $3d_{3/2}$, Ni $2p_{3/2}$, and Ni $2p_{1/2}$, regions of fresh catalysts.

Finally, La 3d 5/2 and its satellite were located at 834.9–836 and 838.5–839.7 eV, and 3d 3/2 and its satellite at 852.5–853 and 856.5–856.9 eV. However, it was not possible to identify La 3d 3/2 in those catalysts whose active metal is Ni, in the same way that the Ni content cannot be quantified. This is due to the superposition with the Auger line of Ni 2p 3/2 and La 3d 3/2 in the case of the catalyst 13Ni/14La-Al_2O_3 and 1Ru-13Ni/14La-Al_2O_3. Nonetheless, the Ni 2p 3/2 corresponding triplet moves toward lower bond energy, while the La 3d 3/2 doublet increases its bond energy, producing the overlapping of the corresponding peaks, confirming the interaction that occurs between La^{3+} and Ni^{2+} [29].

According to the results shown in the spectra represented in Figure 7, a lower proportion of Ni^0 than of NiO is observed in 13Ni/10Mg-Al_2O_3 catalyst, after being reduced in

situ. This can be justified by a higher ease for the oxidation of this catalyst, compared to the rest of the analyzed catalysts. The introduced magnesium interacts with the nickel forming a solid solution difficult to reduce [56]. After its use in the reaction, the complete oxidation of the nickel present in the catalysts is observed, raising the proportion of oxygen present, as shown in Table 3. This increment is especially significant in catalysts with Ca and Ru-La in their composition, assuming an increment of more than 10%. This increment in the oxygen amount is compensated by a reduction in the same proportion of the Al content in 1Ru-13Ni/14La-Al_2O_3 and 1Ru/14La-Al_2O_3 catalysts, and a significant reduction in the proportion of the secondary metal in 13Ni/10Ca-Al_2O_3 and 1Ru-13Ni/14La-Al_2O_3 catalysts (Figure 8). This is due to metal sintering, which produces an agglomeration in deeper layers of the catalyst. On the other hand, although the increment in the proportion of oxygen is not as marked in 13Ni/14Ce-Al_2O_3 and 13Ni/14La-Al_2O_3 catalysts, the reduction in the proportion of Al is up to 9%. Finally, it is necessary to highlight the increase that occurs in the proportion of Ni after its use in the reaction, in 13Ni/14Ce-Al_2O_3 and 13Ni/10Ca-Al_2O_3 catalysts, raising the proportion to double its value. Something similar happens with Ru in 1Ru/Al_2O_3 catalyst.

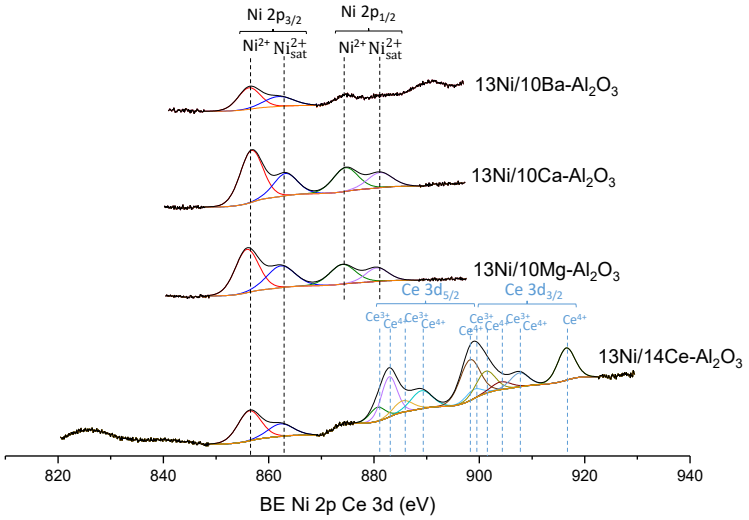

Figure 7. XPS spectra of Ni $2p_{3/2}$, Ni $2p_{1/2}$, Ce $3d_{5/2}$, and Ce $3d_{3/2}$ regions of used catalysts.

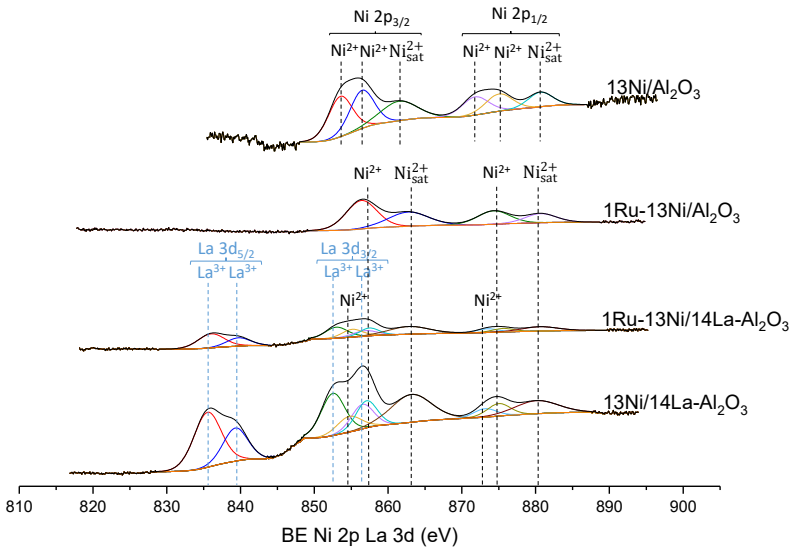

Figure 8. XPS spectra of La $3d_{5/2}$, La $3d_{3/2}$, Ni $2p_{3/2}$, and Ni $2p_{1/2}$ regions of used catalysts.

Table 3. Surface atomic values obtained by XPS analysis of the different catalysts studied.

	Fresh Catalyst					Used Catalyst				
	Al (%)	**O (%)**	**Ni (%)**	**Ru (%)**	**M (%)**	**Al (%)**	**O (%)**	**Ni (%)**	**Ru (%)**	**M (%)**
$13Ni/Al_2O_3$	40.4	56.5	2.7	–	–	37.7	59.1	2.6	–	–
$1Ru\text{-}13Ni/Al_2O_3$	36.9	58.3	3.2	–	–	35.9	60.6	2.7	0.3	–
$1Ru\text{-}13Ni/14La\text{-}Al_2O_3$	38.6	57.0	*	–	4.4	24.5	69.8	3.9	–	1.8
$13Ni/14La\text{-}Al_2O_3$	35.7	60.3	*	–	3.4	26.7	64.9	5.3	–	3.1
$13Ni/10Ba\text{-}Al_2O_3$	32.7	59.2	2.1	–	6.0	28.9	62.9	2.9	–	5.3
$13Ni/10Ca\text{-}Al_2O_3$	27.7	55.2	3.8	–	13.4	21.2	65.5	6.5	–	6.8
$13Ni/10Mg\text{-}Al_2O_3$	33.3	55.6	4.8	–	6.3	30.6	58.1	5.2	–	6.1
$13Ni/14Ce\text{-}Al_2O_3$	32.3	60.8	1.9	–	5.1	23.7	67.5	4.2	–	4.5
$1Ru/14La\text{-}Al_2O_3$	38.1	57.3	–	0.6	3.5	28.5	67.0	–	0.7	3.1
$1Ru/Al_2O_3$	42.1	55.9	–	0.5	–	40.2	58.2	–	1.1	–

* Presence of Ni cannot be quantified (2p line of Ni overlapped with 3d line of La).

The XPS results show that the Al present in used catalysts is found primarily as aluminate. The aluminate is attached to the active metal in its oxidized form, giving rise to a strong interaction. Due to the effect of high temperature and the action of H_2S, it is possible that the migration of the strongly oxygen-bound metal from the aluminate to the surface occur. Despite the increased exposure of the metal, its interaction with the support is likely to block its catalytic capacity. Due to the strong structural change, despite the removal of the H_2S, the catalyst will probably not recover its activity.

3.1.6. XRD

The identification of the main crystalline species was possible through the study of the XRD patterns presented in Figures 9 and 10, corresponding to the XRD patterns of the fresh and used catalysts studied, respectively. The γ-Al_2O_3 support exhibits its diffraction peaks at 37.5°, 44.5°, and 67.4° mainly, corresponding to the crystal planes of (331), (400) and (440), respectively [63,64]. Peaks at 19.7° (111), 34° (220), 57° (422), 61° (511), and 85° (444) can also be used for the identification of the alumina, although they are more difficult to detect specially in the presence of other metals [63,64]. The diffraction peaks of the support observed in the XRD pattern after using the catalysts in the methane reaction up to 773 K, with a current containing H_2S, do not show significant variations.

The diffraction peaks obtained before and after the reaction stage coincide in the same position and without variation of the determined crystal size. In the case of metal promoters, Ni and Ru are in their metallic form both in the reduced fresh and used catalysts, their oxidized form not being detected. Ni peaks are observed at 44.5° (111), 51.6° (200), and 76.7° (220) [17]. In the case of Ru, the main peak is shown at 44.2° (101), the peaks of positions 38.5° (100), 42.3° (002), 78.6° (103), and 84.9° (004) also being part of its pattern [65,66]. Due to the low amount of Ru added to the catalysts, the peaks of this metal disappear [67] in the presence of other promoters, such as Ni in this case. In the presence of the support, it is possible to identify some peaks overlapped by those of the support, especially at 44.2°. This is the only peak located in the presence of La as a support modifier. The lanthanum detected in the XRD pattern is the associated one with the support, in the form of $Al_{22}La_2O_{36}$ and La_3Al, the La_2O_3 phase cannot be identified, which implies its high dispersion on the surface of the support [35]. After the reaction step, the La_2O_3 dispersed into the $13Ni/14La\text{-}Al_2O_3$ catalyst is transformed into the $La_2O_2CO_3$ species. In the rest of the catalysts other La compounds interacting with the support were not identified, remaining as La_2O_3 dispersed in the support.

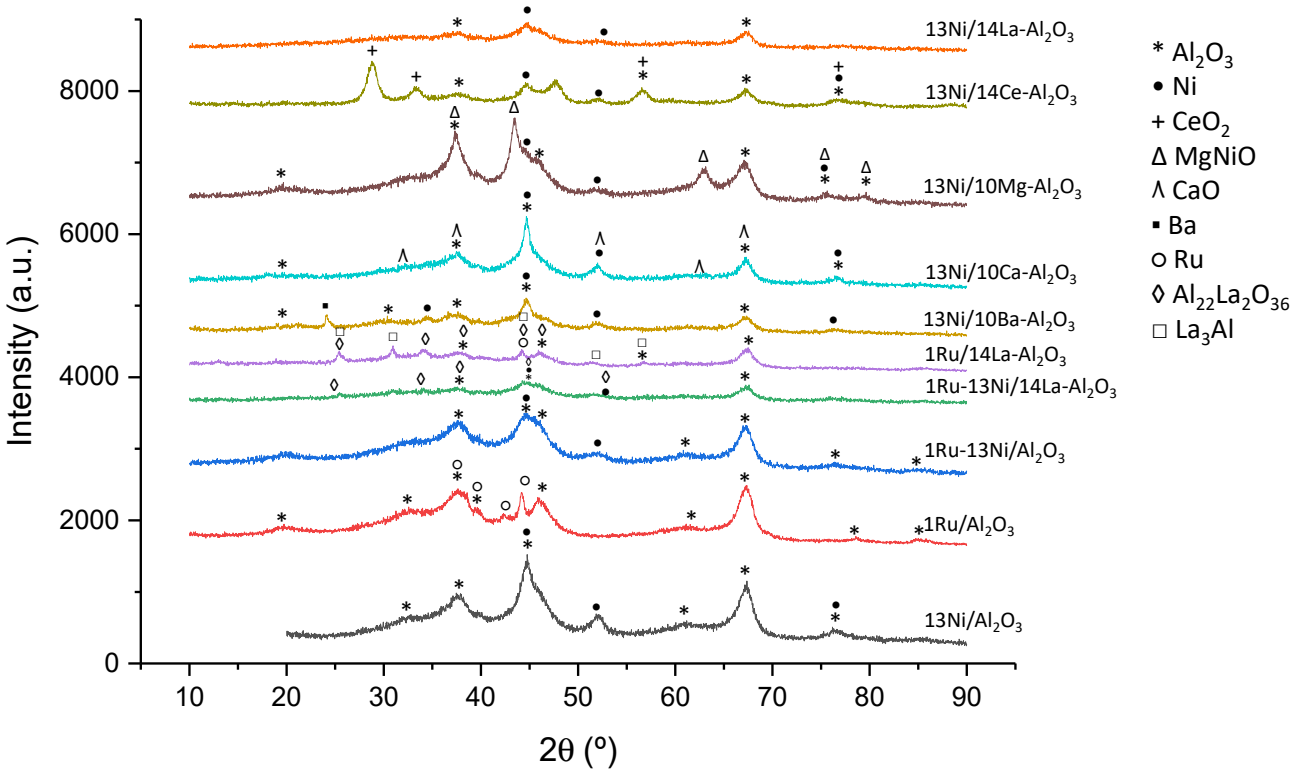

Figure 9. XRD patterns of bi- and monometallic fresh-reduced catalysts supported over Al_2O_3.

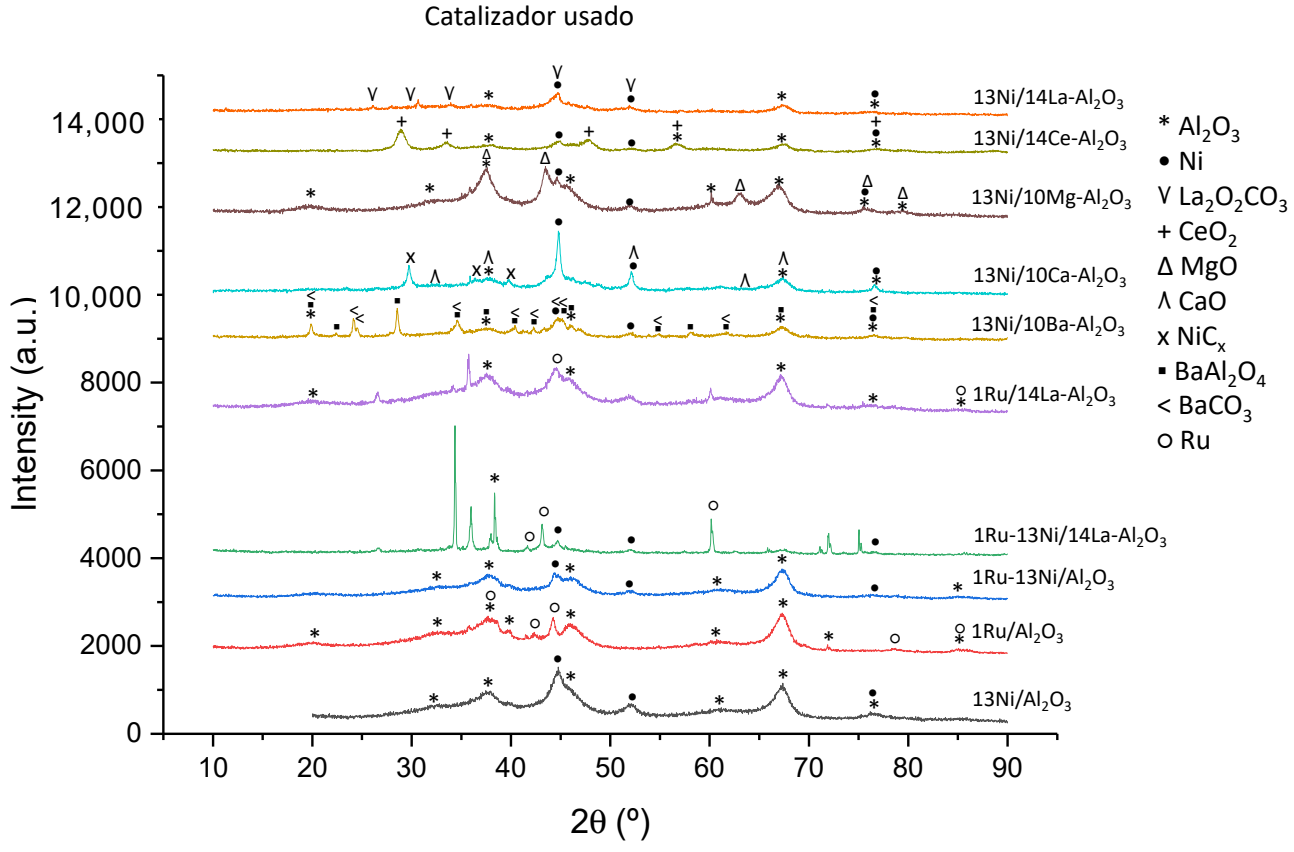

Figure 10. XRD patterns of bi- and monometallic used-reduced catalysts supported over Al_2O_3.

The addition of La, Ce, and Ba to the Ni/Al_2O_3 catalysts produces the damping of the Ni reflection peaks, due to the dispersion of the metal in the support [17,28,29]. The catalyst with Ce has a similar XRD pattern before and after participating in the reaction, identifying the diffraction peaks of CeO_2 in both spectra.

The XRD patterns of the alkaline earth studied in the reduced catalysts show the metals in their metallic or oxidized form: Ba, CaO, and MgNiO. After the reaction, the spectrum of the Mg hardly changes, identifying $Mg_{0·4}Ni_{0·6}O$ present in fresh catalyst in the form of MgO in used catalyst. Calcium remains as CaO, which, as in the catalyst before the reaction, is difficult to identify, due to the coincidence of the peaks that allow its identification with those of the support, much more abundant. However, it is possible to identify in this case the nickel carbide that appears, with the reduction in the intensity of the Ni peaks, as a result of the disappearance of part of the Ni to yield NiCx.

Compared to the previous ones, barium is transformed in the reaction stage into two different compounds: $BaCO_3$ and $BaAl_2O_4$. These species exhibit certain peaks represented in Figure 10, with low intensity, which implies a moderate formation of these elements.

The 2θ position of the diffraction peaks of the XRD patterns determined by X-ray diffraction for the fresh and reduced catalysts (Figure 9), and for the used catalysts (Figure 10) are collected in Table 4 and contrasted with the bibliography.

Table 4. XRD peaks for the metallic species of the catalysts analyzed, determined graphically and contrasted with the bibliography.

Metallic Species	JCPDS Code	Value (2θ)	Bibliography
Al_2O_3	077-0396	19.7, 34, 37.5, 44.5, 57, 61, 67.4, 85	[63,64]
Ni	087-0712	44.5, 51.6, 76.7	[17]
Ru	088-1734	38.5, 42.3, 44.2, 78.6, 84.9	[65,66]
Ba	006-0235	24.1, 34.5	[28,53]
CaO	086-0402	32.2, 37.3, 53.8, 64.1, 67.3	[34,68]
$Mg_{0·4}Ni_{0·6}O$	034-0410	37.4, 43.5, 63, 75.5, 79.4	[69,70]
MgO	087-0653	37.5, 43.5, 63, 75.7, 79.2	[69,70]
CeO_2	075-0076	28.9, 33.4, 47.7, 56.6, 76.8	[65,71]
$Al_{22}La_2O_{36}$	028-0502	25.8, 34.1, 37.5, 44.5, 45.9, 51.6	[29]
$LaAlO_3$	031-0022	25.3, 30.8, 44.1, 51.3, 56.7	[29]
$BaAl_2O_4$	017-0306	19.7, 22.2, 28.4, 34.5, 37.5, 40.3, 42.2, 45.1, 45.9, 54.7, 58, 61.5, 67.2, 76.4	[34,53,72]
$BaCO_3$	005-0378	19.7, 24, 24.4, 34.5, 40.3, 42.2, 44.6, 45.1, 54.7, 61.5, 76.4	[34,72]
$La_2O_2CO_3$	025-0424	26, 30.5, 33.74, 44.6, 51.82	[73]

The average crystallite size of species present in the catalysts was estimated employing the Scherrer equation and a significant peak of the XRD patterns. The peaks used and the crystal size determined are collected in Tables 1 and 5. After the reaction stage, an increase in crystal size is observed in all the species analyzed, with the exception of Ru. The increase in Ni crystal size is a consequence of the sintering that takes place in the catalyst.

Table 5. Crystal size determined by Scherrer equation and a diffraction peak of XRD pattern for the species present in the reduced and used in reaction catalysts.

Species	Peak Position (°)	Crystal Size Approximation of Reduced Catalyst (nm)	Crystal Size Approximation of Used Catalyst (nm)
Ru	44.2	20	5 (20 for the $1Ru/Al_2O_3$)
Ni	51.9	<5	15

3.2. Activity Tests

The catalytic activity was measured as the CH_4 yield obtained for each temperature analyzed in the CO_2 methanation. The activity study was carried out primarily for Ni-based catalysts supported on alumina, and modified with lanthanides (La or Ce, 14 wt%), and alkaline earth metals (Ba, Ca, or Mg, 10 wt%). This study was done for temperatures between 573 and 773 K, with a quantity of catalyst of 200 mg, corresponding to a weight hourly space velocity (WSHV) of 38.3 h^{-1}. The results obtained for the methane yield are reported in Figure 11.

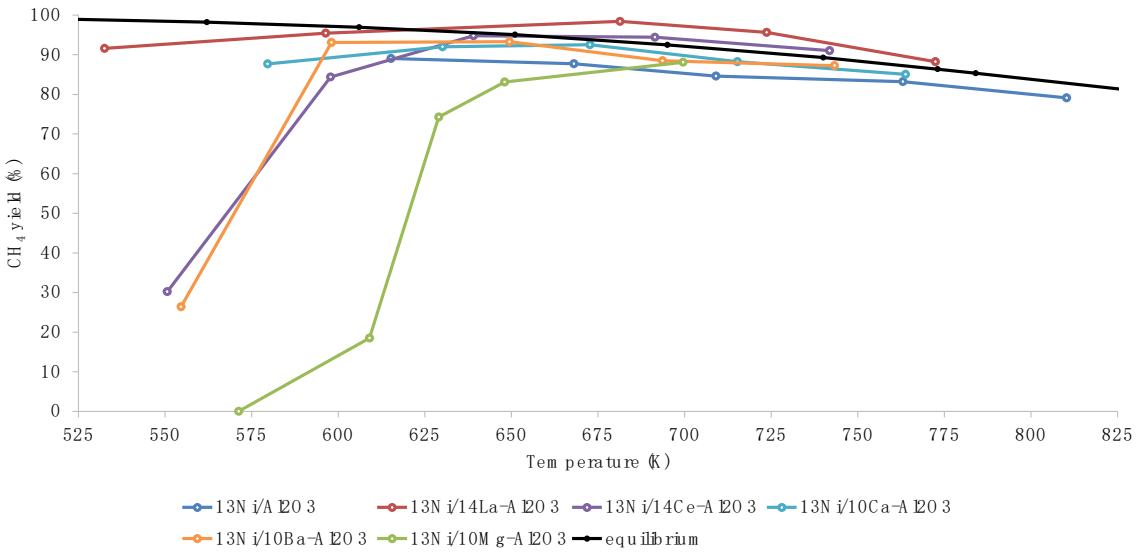

Figure 11. Methane yield obtained for 200 mg for catalysts supported on alumina.

All the catalysts studied reaches 100% CH_4 selectivity at the experimental conditions, detecting only trace amounts of CO as a by-product. The maximum methane yield value was reached and established by the thermodynamic equilibrium in the temperature range. In the case of 13Ni/10Mg-Al_2O_3 catalyst, it needed a higher temperature to reach the equilibrium value, 700 K. This was followed by 13Ni/14Ce-Al_2O_3 and 13Ni/10Ba-Al_2O_3 catalysts, which reached it at 639 K and 598 K, respectively. The rest of the catalysts started from the thermodynamic equilibrium value. To facilitate the comparison, the amount of catalyst was reduced to 125 mg to increase the WSHV value to 60.8 h^{-1}.

On the other hand, the resistance of the catalysts to H_2S poisoning was previously evaluated. For this, 50 ppm of H_2S were introduced with the reaction gases, determining the time necessary for the complete deactivation of the catalysts, results are represented in Figure 12.

The catalysts with the greatest resistance to deactivation were those modified with lanthanides (13Ni/14La-Al_2O_3 and 13Ni/14Ce-Al_2O_3), requiring up to 110 min for complete deactivation. On the contrary, those catalysts modified with alkaline earth deactivated the first ones, starting with 13Ni/10Ba-Al_2O_3 at 40 min, followed by 13Ni/10Mg-Al_2O_3 at 50 min and finally 13Ni/10Ca-Al_2O_3 at 60 min. The 13Ni/Al_2O_3 catalyst showed an intermediate resistance, lower than those modified with lanthanides, deactivating at 70 min.

The results obtained using 125 mg of catalyst, and a temperature range between 498 and 573 K, are shown in Figure 13.

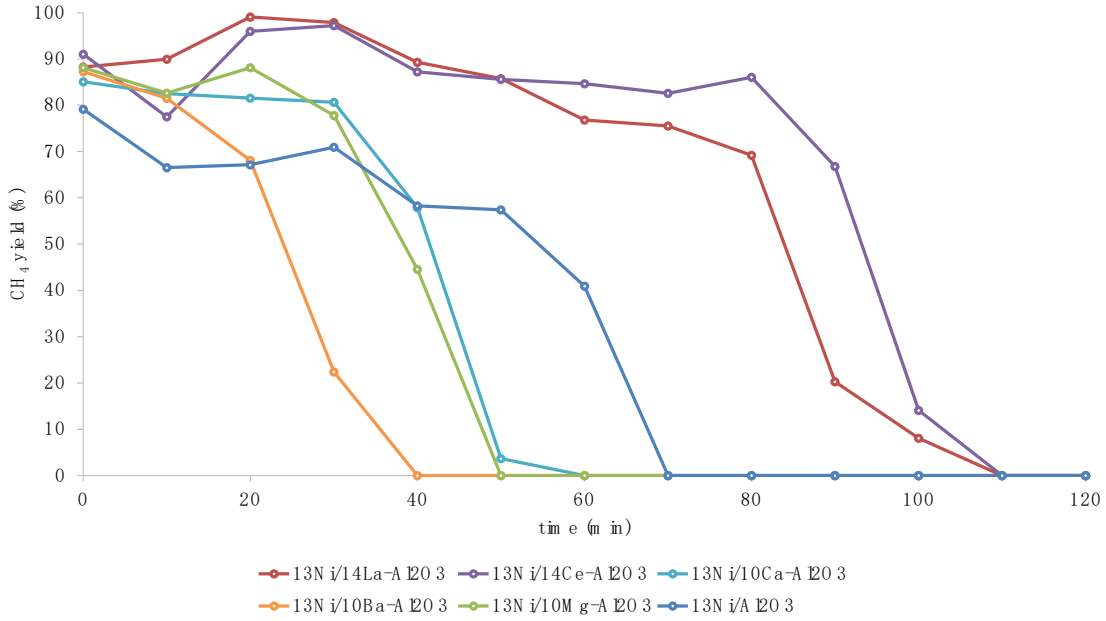

Figure 12. Catalysts deactivation for 200 mg of catalysts supported on alumina due to 50 ppm of H_2S at 773 K.

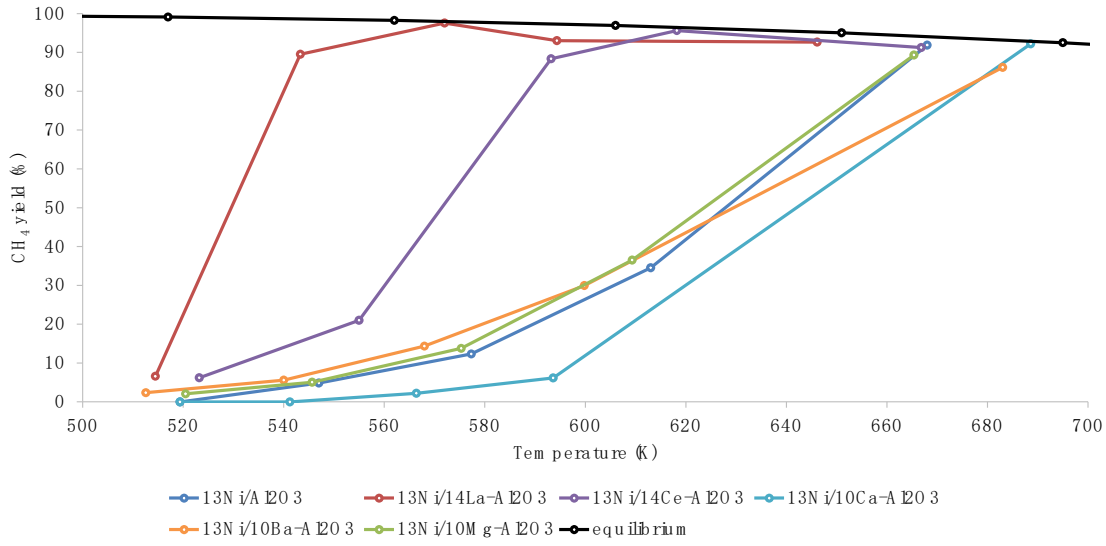

Figure 13. Methane yield obtained for 125 mg of catalysts supported on alumina.

As expected, the reduction in the amount of catalyst (or increase in WSHV) increased the temperature necessary to achieve the maximum performance established by thermodynamic equilibrium. In the case of supports modified with alkaline earth metals (13Ni/10Ba-Al_2O_3, 13Ni/10Ca-Al_2O_3, and 13Ni/10Mg-Al_2O_3) and the reference catalyst (13Ni/Al_2O_3), the activity increased progressively until reaching the thermodynamic equilibrium at the highest temperature studied. 13Ni/Al_2O_3 and 13Ni/10Mg-Al_2O_3 catalysts reached a yield of 92 and 89% at 668 and 665 K respectively, while 13Ni/10Ba-Al_2O_3 and 13Ni/10Ca-Al_2O_3 catalysts reached 86 and 90% at 683 and 688 K, respectively. Moreover, according to the ICP characterization results, these catalysts presented the lower Ni content. The catalysts modified with lanthanide metals achieved the equilibrium yield at lower temperatures. 13Ni/14Ce-Al_2O_3 reached a methane yield of 96% at 618 K. However, catalyst 13Ni/14La-Al_2O_3 at 543 K yielded a 90%, reaching up to 98% at 572 K with a medium content of Ni measured by ICP. As a previous conclusion, cerium and specially lanthanum

addition enhanced the activity to methane with respect to Ce or La-free and alkaline earth modified catalysts.

The high yields of catalyst 13Ni/14La-Al_2O_3 at low temperatures, would allow the methanation of a greater flow of reaction gases or, the use of a smaller amount of catalyst. Therefore, the feasibility of this hypothesis is compared in the case of catalyst 13Ni/Al_2O_3, for different amounts of catalyst. Figure 14 compares the methane yield of catalyst 13Ni/Al_2O_3 for 200 mg of catalyst and 38.3 h^{-1} of WSHV; 125 mg and 60.8 h^{-1}; and 60 mg and 128.75 h^{-1}.

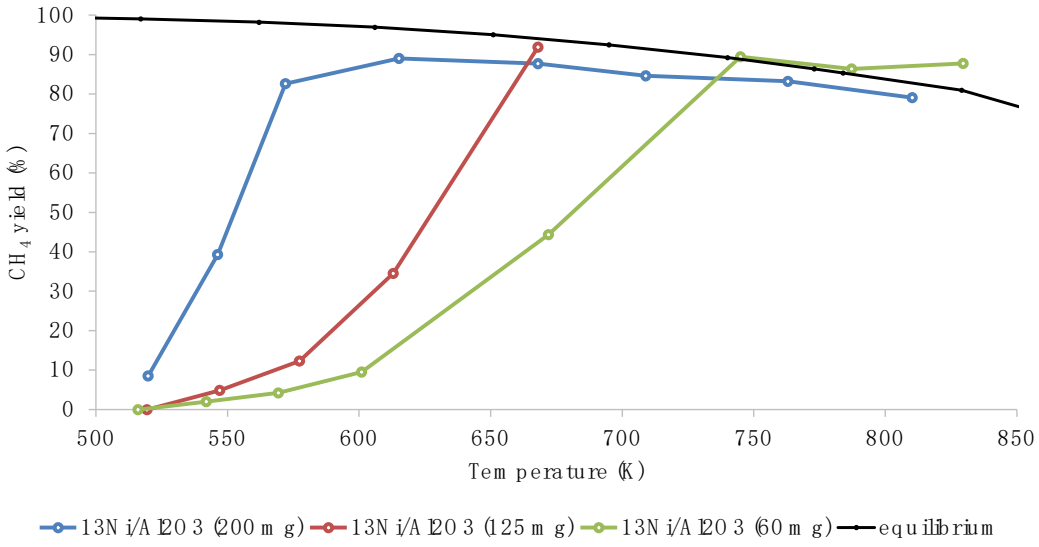

Figure 14. Comparison of methane yield for different amounts of 13Ni/Alumina catalyst.

The decrease in the amount of catalyst used resulted in an increase in the temperature at which the thermodynamic equilibrium is reached, as previously observed. With a load of 200 mg of catalyst in the reactor, the equilibrium temperature was reached at a temperature of 572 K, while for 125 mg, the temperature needs to be raised to 668 K. Finally, for an amount of 60 mg the equilibrium temperature is not reached until 745 K was reached.

Thus, 60 mg of catalyst (128.75 h^{-1}), and a temperature range between 598 and 773 K, was used to compare the improvement in the activity of catalysts based on Ru-, Ni-, and La-supported on alumina. Results are shown in the Figure 15.

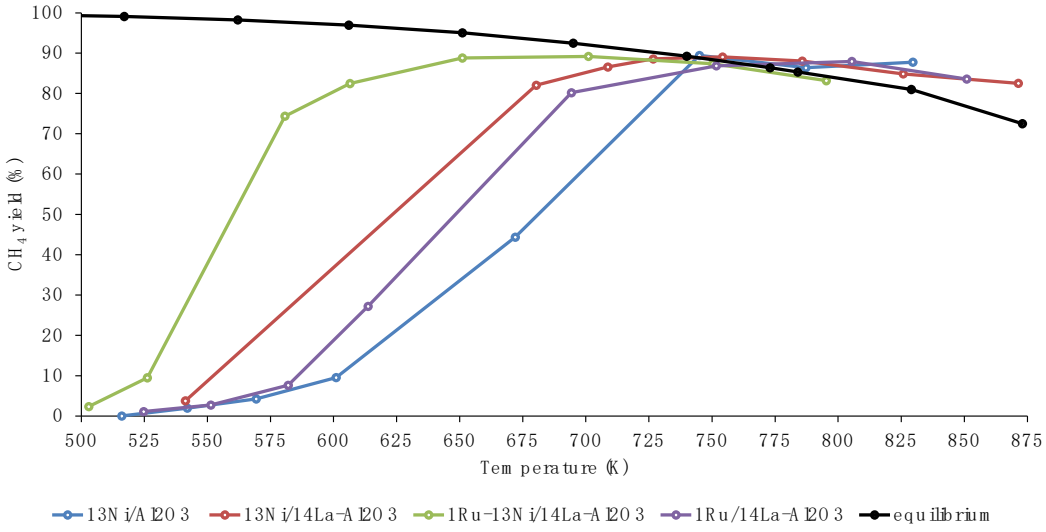

Figure 15. Methane yield obtained for 60 mg of catalysts supported on alumina.

Catalyst 13Ni/Al_2O_3, as seen in Figure 15, achieved a maximum methane yield of 90% at 745 K. The addition of La reduced the value of the temperature necessary to reach a yield of 82% to 680 K (and 89% at 727 K). Substituting nickel for a noble metal, such as Ru, at a nominal content of 1 wt% with La-modified support, it reached 80% yield at 694 K. The difference between the 1Ru/14La-Al_2O_3 and 13Ni/14La-Al_2O_3 catalysts is quite small, the Ni-containing catalyst being slightly better. The incorporation of Ru into the 13Ni/14La-Al_2O_3 catalyst produced a clear improvement in the methanation rate with respect to the other catalysts, despite the decrease in the amount of Ru incorporated as observed in the ICP results. At 581 K, the methane yield reached by this catalyst was 74%, reaching a maximum value of 89% at 651 K. Therefore, although the contribution of Ru appears to be similar to that of Ni, the effect of Ni is greater than that of Ru, especially in combination.

Once the activity of the catalysts in the methanation reaction has been studied, as for catalysts modified with alkaline earth metals, the resistance of the catalysts to poisoning in the presence of 50 ppm of H_2S is determined. The results obtained for the deactivation of the catalysts are presented in Figure 16.

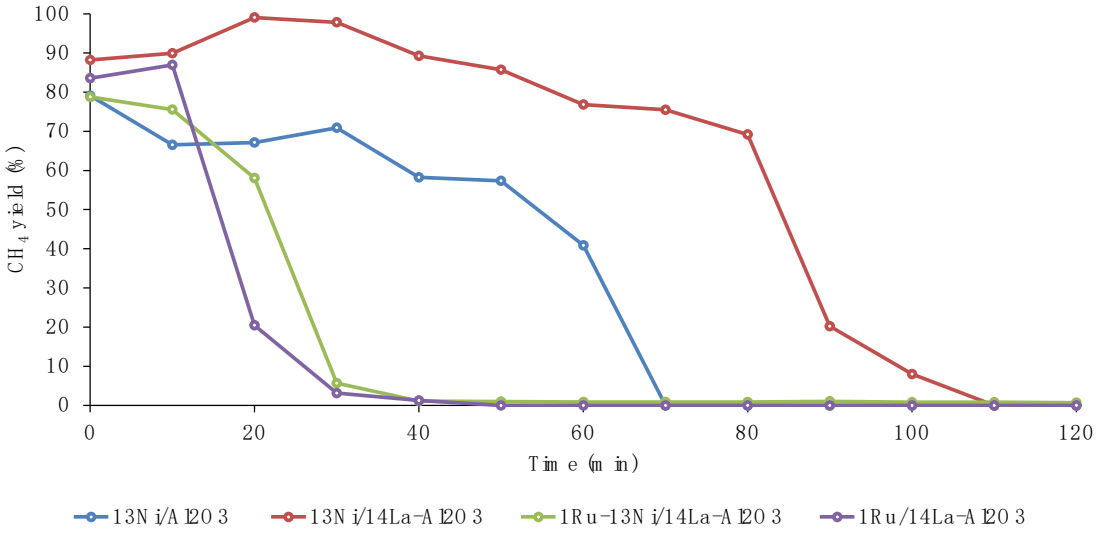

Figure 16. Catalysts deactivation for 60 mg of catalysts supported on alumina due to 50 ppm of H_2S at 773 K.

The addition of 50 ppm of H_2S to the reaction gases reduced the activity of catalysts containing Ru faster than those containing only Ni. Thus, 1Ru/14La-Al_2O_3 and 1Ru-13Ni/14La-Al_2O_3 were deactivated in 40 min. The addition of La to Ni, in addition to improving the methane activity of the catalysts, improved its resistance to H_2S poisoning, lengthening the deactivation from 70 min of catalyst 13Ni/Al_2O_3 to 110 min of catalyst 13Ni/14La-Al_2O_3.

After deactivation of the catalysts in the presence of H_2S, the methane yield of the catalysts was studied by eliminating H_2S from the feed at 773 K. In all the cases analyzed, the catalysts did not recover the activity.

Finally, catalysts were regenerated, employing a mixture of 3% O_2 and N_2, in order to eliminate the coke or the sulfur that may block the catalytic action of the catalysts. Then, the catalysts were reactivated by reduction with H_2. The recovered catalyst was used in a reaction stage, at 773 K. The catalyst activity was observed as methane yield was not recovered [37,74]. During the reaction or deactivation stage, CO could have appeared as a by-product of the reverse water gas shift reaction, but it could also appear by the partial oxidation of the coke in the regeneration. In spite of everything, the presence of this gas was not detected.

3.3. Discussion

The use of noble metals as catalyst in the methanation reaction has been extensively studied in the literature, demonstrating high efficiency with greater thermal stability, as observed in Garbarino's work [13]. Despite showing that the performance achieved for nickel-based catalysts is not as high as that obtained for ruthenium, the performance is high and with easier activation [10,13,50]. In order to complement the advantages of nickel and ruthenium as active metals in the methanation reaction, it was co-impregnated on the support. Thus, it was verified that the addition of ruthenium and nickel improved the performance of the catalyst, improving thermal stability and facilitating its activation, as determined in Liu's work [75].

The incorporation of alkaline earth metals and lanthanides that modified the support has been shown to reach higher activity, improving the interaction between support and metal [28,29]. The incorporation of alkaline earth metals has improved the activity of the nickel catalyst, but less significantly than adding lanthanide metals. The alkaline earth metals could increase the alkalinity of the catalyst, resulting in a reduction in the number of acid centers with low and medium strength and an increase in the basic centers with medium and high strength. This results in less interaction of nickel with alumina than observed for lanthanide-modified catalysts, which favors catalyst activity. Taking into account the obtained results for the alkaline earth metals catalyst, the general properties (as textural properties) analyzed are similar to those of the monometallic catalyst, concluding with a similar activity. However, it is necessary to specify that according to H_2-TPR results, the addition of barium facilitated the activation of the catalyst, contrary to what was observed for calcium and magnesium. These results are in a good agreement with those obtained in Liang's work [28], in which little improvement was observed in the catalytic activity of the nickel catalyst in the presence of Ca or Mg. The methane yield determined for catalysts of Ni and Ni with 5% of Ca or Mg were around 50% in these cases at 623 K. However, the addition of Ba (from 1 to 7.5%) showed a reduction in the temperatures at which the catalyst is active for the methanation reaction, reaching a yield of 80% at 623 K, incorporating in that case 7.5% of Ba. The differences in performance obtained in our catalysts using 125 mg of catalyst instead of 500 mg are less significant, reaching a methane yield close to 50% in all of them.

A significant improvement in the activity of the nickel catalyst was produced by the addition of lanthanide metals, especially with La. Ce was incorporated as non-stoichiometric CeO_2, surface reducible metal centers of CeO_2, and bulk reducible metal centers of CeO_2 [52]. Ce^{4+} from CeO_2 interacted with Ni, as observed in the H_2-TPR analysis, improving its reducibility which facilitated its activation. There is a strong interaction with Ni, determined by XRD, which contributes to the strengthening of the interaction with the support and improved the dispersion of the metal on its surface, increasing the catalytic activity of the catalyst. Previous studies from our laboratory [19] have shown that the addition of cerium promotes the formation of active species, of nickel-aluminate spinel-like structure, which improves the yield of methane up to 75% at 647 K for the 13Ni/6Ce-Al_2O_3 catalyst, a temperature for the Ni catalyst of 723 K being necessary to achieve the same performance.

The addition of lanthanum, as well as cerium, produced an improvement in the reducibility of the catalyst that facilitated its activation, increasing the amount of free NiO dispersed on the surface of the alumina [29,45,51]. This was caused due to a weakening of the interaction between NiO and the support by destroying partially metastable Ni-Al mixed oxide phase, caused by La incorporation [45,51]. On the other hand, La interacted with the strongest acid and basic centers of alumina, through La^{3+}-O^{2-} pairs, as was observed by NH_3-TPD, increasing the density of acid centers of higher strength [41]. La contribution was especially important in Ru and Ni catalysts, in which the number of acid centers increased more significantly. It implied a higher dispersion of the active metals on the surface of the support, as verified in the results obtained by XRD. In this analysis, La was dispersed, interacting with the support, forming species such as $Al_{22}La_2O_{36}$ and

La_3Al. The Ni and/or Ru centers, facilitated by the structures made up of La and alumina, were dispersed over the surface. It helped to increase the activity of the catalyst in the methanation reaction, as it was deduced from the previous analyses and it was verified in the activity results. The increase in the yield to methane was observed from 34% for $13Ni/Al_2O_3$ to 65% for $13Ni/14La\text{-}Al_2O_3$ at 650 K, just like in Garbarino's work [29], in which this important increase in activity was observed by the addition of lanthanum to the nickel catalyst, raising the yield from 72 to 90% to 625 K.

The most outstanding observation deduced from our work was the importance of the incorporation of Ru as a promoter, together with Ni, for the improvement of the activity of the catalyst in the reaction. An increase in yield from 65% for $13Ni/14La\text{-}Al_2O_3$ to 90% for $1Ru\text{-}13Ni/14La\text{-}Al_2O_3$ was observed at 650 K. This increase was probably due to the synergistic effect that occurs between Ru and Ni, due to the interaction that takes place between said metals as observed in H_2-TPR and verified with the Liu's work [75]. Ru dispersed as RuO_2 and RuO_x across the surface of the support in contact with the NiO present, being able to produce Ru-Ni bimetallic particles [50]. Ru decreased the reduction temperature of Ni, favoring its activation and facilitating its dispersion, which led to increased activity as shown, and contributing to this effect La.

Regarding the resistance of the catalyst to poisoning with H_2S, it was observed that the incorporation of alkaline earth metals exposed to a greater extent the active centers of the metal to the H_2S, facilitating its deactivation. The incorporation of lanthanide metals improved resistance to H_2S poisoning, due to the strong interaction between nickel and Ce or Ni and La, which makes it difficult to approach and block these centers, by reducing their affinity. Ni is more resistant to poisoning than Ru, which, in the presence of H_2S, was rapidly deactivated due to its greater affinity for this element (more electronegative) than for H_2.

Once the catalyst was deactivated, the activity was not recovered, due to the morphological change that follows in the catalyst, in view of the analyzed XPS and XRD results. An increase in the amount of oxygen and nickel at the catalyst surface was observed, along with a reduction for aluminum. This could involve the formation of an aluminate structure that covers the nickel, blocking the access of the reagents and their interaction, as the presence of sulfur in their content was not determined. Under these conditions, the catalyst could completely lose its activity, preventing its recovery.

4. Conclusions

The conclusions summarized below have been deduced from the development of this work.

The addition of Ba, Ca, or Mg in a proportion of 10% does not improve the activity of the nickel catalyst in a significant way, probably due to the slight differences obtained in the physico-chemical characterization.

The addition of 14% of Ce improves the reducibility and dispersion of nickel, as suggested in the characterization, by facilitating new anchor centers on the surface of the support, which improves its activity at lower temperatures.

La (incorporated in a proportion of 14%) shows a strong interaction with alumina, which facilitates the incorporation of Ni. Greater dispersion and higher density of active centers were obtained, composed of easily reducible NiO species, which probably were responsible of the improvement in activity at lower temperatures.

La-doped Ni/Al_2O_3 catalyst is competitive with Ru/Al_2O_3 catalyst. The incorporation of ruthenium as a promoter produces a strong interaction with nickel, increasing its catalytic activity, reinforced by lanthanum, which increases dispersion and reducibility reaching a 90% methane yield at 650 K for a WSHV of 128.75 h^{-1}.

The strong interaction between La or Ce with Ni hinders the exposure and access of the H_2S to the active centers of the metal.

The high temperatures (773 K) and the action of the H_2S produced the complete deactivation of the catalysts studied. A possible change in the morphology of the catalyst

was determined, whereby the oxygenated structures of the support and the metals they incorporate, block access to the metal centers of the reagents.

Author Contributions: Conceptualization, D.M.-M., V.L.B., J.M.R. and J.F.C.; methodology, D.M.-M., V.L.B., J.M.R. and J.F.C.; software, D.M.-M.; validation, D.M.-M., V.L.B., J.M.R. and J.F.C.; formal analysis, D.M.-M.; investigation, D.M.-M.; resources, V.L.B., J.M.R. and J.F.C.; data curation, D.M.-M., V.L.B., J.M.R. and J.F.C.; writing—original draft preparation, D.M.-M.; writing—review and editing, D.M.-M.; visualization, D.M.-M., V.L.B., J.M.R. and J.F.C.; supervision, D.M.-M.; V.L.B., J.M.R. and J.F.C.; project administration, V.L.B., J.M.R. and J.F.C.; funding acquisition, V.L.B., J.M.R. and J.F.C. All authors have read and agreed to the published version of the manuscript.

Funding: This research received no external funding.

Acknowledgments: This research was supported by the University of the Basque Country (UPV/EHU) and the Basque Government (IT993-16), Spanish Ministry of Economy and Competitiveness (ENE2017-82250-R), and the European Union through the European Regional Development Fund (FEDER). The authors thank for technical and human support provided by SGIker of UPV/EHU and European funding (ERDF and ESF).

Conflicts of Interest: There are no conflicts to declare.

References

1. United Nations. Climate Change. Available online: https://www.un.org/en/sections/issues-depth/climate-change/index.html (accessed on 24 September 2019).
2. Tuckett, R. Greenhouse Gases. In *Reference Module in Chemistry, Molecular Sciences and Chemical Engineering*; Elsevier: Amsterdam, The Netherlands, 2018; p. B9780124095472140000. [CrossRef]
3. Khapre, A.; Jaiswal, A.; Kumar, S. Utilizing the greenhouse effect as a source to produce renewable energy. In *Reference Module in Materials Science and Materials Engineering*; Elsevier: Amsterdam, The Netherlands, 2019; pp. 835–843.
4. Allen, M.R.; Dube, O.P.; Solecki, W.; Aragón-Durand, F.; Cramer, S.; Humphreys, W.; Kainuma, M.; Kala, J.; Mahowald, N.; Mulugetta, Y.; et al. *Global Warming of 1.5 °C. An IPCC Special Report on the Impacts of Global Warming of 1.5 °C Above Pre-Industrial Levels and Related Global Greenhouse Gas Emission Pathways, in the Context of Strengthening the Global Response to the Threat of Climate Change, Sustainable Development, and Efforts to Eradicate Poverty*; IPCC: Geneva, Switzerland, 2018.
5. European Commission. Communication from the Commission. A Clean Planet for All, (2018). Available online: https://eur-lex.europa.eu/legal-content/EN/TXT/HTML/?uri=CELEX:52018DC0773&from=EN (accessed on 24 September 2019).
6. Yaashikaa, P.; Kumar, P.S.; Varjani, S.J.; Saravanan, A. A review on photochemical, biochemical and electrochemical transformation of CO_2 into value-added products. *J. CO_2 Util.* **2019**, *33*, 131–147. [CrossRef]
7. Kumar, S.S.; Himabindu, V. Hydrogen production by PEM water electrolysis—A review. *Mater. Sci. Energy Technol.* **2019**, *2*, 442–454. [CrossRef]
8. Esa, Y.A.M.; Sapawe, N. A short review on carbon dioxide (CO_2) methanation process. *Mater. Today Proc.* **2020**, *31*, 394–397. [CrossRef]
9. Moioli, E.; Gallandat, N.; Züttel, A. Model based determination of the optimal reactor concept for Sabatier reaction in small-scale applications over Ru/Al_2O_3. *Chem. Eng. J.* **2019**, *375*, 121954. [CrossRef]
10. Muroyama, H.; Tsuda, Y.; Asakoshi, T.; Masitah, H.; Okanishi, T.; Matsui, T.; Eguchi, K. Carbon dioxide methanation over Ni catalysts supported on various metal oxides. *J. Catal.* **2016**, *343*, 178–184. [CrossRef]
11. Kuzmenko, D.; Nachtegaal, M.; Copéret, C.; Schildhauer, T. Molecular-level understanding of support effects on the regenerability of Ru-based catalysts in the sulfur-poisoned methanation reaction. *J. Catal.* **2019**, *375*, 74–80. [CrossRef]
12. Dreyer, J.A.; Li, P.; Zhang, L.; Beh, G.K.; Zhang, R.; Sit, P.H.-L.; Teoh, W.Y. Influence of the oxide support reducibility on the CO_2 methanation over Ru-based catalysts. *Appl. Catal. B Environ.* **2017**, *219*, 715–726. [CrossRef]
13. Garbarino, G.; Bellotti, D.; Riani, P.; Magistri, L.; Busca, G. Methanation of carbon dioxide on Ru/Al 2 O 3 and Ni/Al 2 O 3 catalysts at atmospheric pressure: Catalysts activation, behaviour and stability. *Int. J. Hydrog. Energy* **2015**, *40*, 9171–9182. [CrossRef]
14. Tada, S.; Ochieng, O.J.; Kikuchi, R.; Haneda, T.; Kameyama, H. Promotion of CO_2 methanation activity and CH4 selectivity at low temperatures over Ru/CeO2/Al_2O_3 catalysts. *Int. J. Hydrog. Energy* **2014**, *39*, 10090–10100. [CrossRef]
15. Beuls, A.; Swalus, C.; Jacquemin, M.; Heyen, G.; Karelovic, A.; Ruiz, P. Methanation of CO_2: Further insight into the mechanism over Rh/γ-Al_2O_3 catalyst. *Appl. Catal. B Environ.* **2012**, *113–114*, 2–10. [CrossRef]
16. Karelovic, A.; Ruiz, P. Mechanistic study of low temperature CO_2 methanation over Rh/TiO2 catalysts. *J. Catal.* **2013**, *301*, 141–153. [CrossRef]
17. Hu, F.; Tong, S.; Lu, K.; Chen, C.-M.; Su, F.-Y.; Zhou, J.; Lu, Z.-H.; Wang, X.; Feng, G.; Zhang, R. Reduced graphene oxide supported Ni-Ce catalysts for CO_2 methanation: The support and ceria promotion effects. *J. CO_2 Util.* **2019**, *34*, 676–687. [CrossRef]

18. Ye, R.-P.; Gong, W.; Sun, Z.; Sheng, Q.; Shi, X.; Wang, T.; Yao, Y.; Razink, J.J.; Lin, L.; Zhou, Z.; et al. Enhanced stability of Ni/SiO2 catalyst for CO_2 methanation: Derived from nickel phyllosilicate with strong metal-support interactions. *Energy* **2019**, *188*, 116059. [CrossRef]
19. García, I.G.; Izquierdo, U.; Barrio, V.; Arias, P.L.; Cambra, J.F. Power-to-Gas: Storing surplus electrical energy. Study of Al 2 O 3 support modification. *Int. J. Hydrog. Energy* **2016**, *41*, 19587–19594. [CrossRef]
20. Zamani, A.; Ali, R.L.; Abu Bakar, W. Optimization of CO_2 methanation reaction over M*/Mn/Cu–Al_2O_3 (M*: Pd, Rh and Ru) catalysts. *J. Ind. Eng. Chem.* **2015**, *29*, 238–248. [CrossRef]
21. Garbarino, G.; Riani, P.; Magistri, L.; Busca, G. A study of the methanation of carbon dioxide on Ni/Al_2O_3 catalysts at atmospheric pressure. *Int. J. Hydrog. Energy* **2014**, *39*, 11557–11565. [CrossRef]
22. Swalus, C.; Jacquemin, M.; Poleunis, C.; Bertrand, P.; Ruiz, P. CO_2 methanation on Rh/γ-Al_2O_3 catalyst at low temperature: "In situ" supply of hydrogen by Ni/activated carbon catalyst. *Appl. Catal. B Environ.* **2012**, *125*, 41–50. [CrossRef]
23. Mihet, M.; Lazar, M.D. Methanation of CO_2 on Ni/γ-Al_2O_3: Influence of Pt, Pd or Rh promotion. *Catal. Today* **2018**, *306*, 294–299. [CrossRef]
24. Ashok, J.; Pati, S.; Hongmanorom, P.; Tianxi, Z.; Junmei, C.; Kawi, S. A review of recent catalyst advances in CO_2 methanation processes. *Catal. Today* **2020**, *356*, 471–489. [CrossRef]
25. Renda, S.; Ricca, A.; Palma, V. Study of the effect of noble metal promotion in Ni-based catalyst for the Sabatier reaction. *Int. J. Hydrog. Energy* **2020**. [CrossRef]
26. Bustinza, A.; Frías, M.; Liu, Y.; Garcia-Bordeje, E. Mono- and bimetallic metal catalysts based on Ni and Ru supported on alumina-coated monoliths for CO_2 methanation. *Catal. Sci. Technol.* **2020**, *10*, 4061–4071. [CrossRef]
27. Trueba, M.; Trasatti, S.P. γ-Alumina as a support for catalysts: A review of fundamental aspects. *Eur. J. Inorg. Chem.* **2005**, *2005*, 3393–3403. [CrossRef]
28. Liang, C.; Hu, X.; Wei, T.; Jia, P.; Zhang, Z.; Dong, D.; Zhang, S.; Liu, Q.; Hu, G. Methanation of CO_2 over Ni/Al_2O_3 modified with alkaline earth metals: Impacts of oxygen vacancies on catalytic activity. *Int. J. Hydrog. Energy* **2019**, *44*, 8197–8213. [CrossRef]
29. Garbarino, G.; Wang, C.; Cavattoni, T.; Finocchio, E.; Riani, P.; Flytzani-Stephanopoulos, M.; Busca, G. A study of Ni/La-Al_2O_3 catalysts: A competitive system for CO_2 methanation. *Appl. Catal. B Environ.* **2019**, *248*, 286–297. [CrossRef]
30. Tsiotsias, A.I.; Charisiou, N.D.; Yentekakis, I.V.; Goula, M.A. The role of alkali and alkaline earth metals in the CO_2 methanation reaction and the combined capture and methanation of CO_2. *Catalysts* **2020**, *10*, 812. [CrossRef]
31. Jomjaree, T.; Sintuya, P.; Srifa, A.; Koo-Amornpattana, W.; Kiatphuengporn, S.; Assabumrungrat, S.; Sudoh, M.; Watanabe, R.; Fukuhara, C.; Ratchahat, S. Catalytic performance of Ni catalysts supported on different CeO2 morphologies for low-temperature CO_2 methanation. *Catal. Today* **2020**. [CrossRef]
32. Meeyoo, V.; Panchan, N.; Phongprueksathat, N.; Traitangwong, A.; Guo, X.; Li, C.; Rirksomboon, T. Low Temperature Methanation of CO_2 on High Ni Content Ni-Ce-ZrOδ Catalysts Prepared via One-Pot Hydrothermal Synthesis. *Catalysts* **2019**, *10*, 32. [CrossRef]
33. Charisiou, N.; Siakavelas, G.; Papageridis, K.; Baklavaridis, A.; Tzounis, L.; Avraam, D.; Goula, M. Syngas production via the biogas dry reforming reaction over nickel supported on modified with CeO 2 and/or La 2 O 3 alumina catalysts. *J. Nat. Gas Sci. Eng.* **2016**, *31*, 164–183. [CrossRef]
34. Maina, S.C.; Ballarini, A.D.; Vilella, J.I.; De Miguel, S.R. Study of the performance and stability in the dry reforming of methane of doped alumina supported iridium catalysts. *Catal. Today* **2020**, *344*, 129–142. [CrossRef]
35. Cai, Z.; Li, J.; Liew, K.; Hu, J. Effect of La2O3-dopping on the Al_2O_3 supported cobalt catalyst for Fischer-Tropsch synthesis. *J. Mol. Catal. A Chem.* **2010**, *330*, 10–17. [CrossRef]
36. Riani, P.; Valsamakis, I.; Cavattoni, T.; Escribano, V.S.; Busca, G.; Garbarino, G. Ni/SiO2-Al_2O_3 catalysts for CO_2 methanation: Effect of La2O3 addition. *Appl. Catal. B Environ.* **2021**, *284*, 119697. [CrossRef]
37. Méndez-Mateos, D.; Barrio, V.L.; Requies, J.M.; Cambra, J.F. A study of deactivation by H2S and regeneration of a Ni catalyst supported on Al_2O_3, during methanation of CO_2. Effect of the promoters Co, Cr, Fe and Mo. *RSC Adv.* **2020**, *10*, 16551–16564. [CrossRef]
38. Franks, G.V.; Meagher, L. The isoelectric points of sapphire crystals and alpha-alumina powder. *Colloids Surf. A Physicochem. Eng. Asp.* **2003**, *214*, 99–110. [CrossRef]
39. Schilhauer, T.J.; Biollaz, S.M.A. Synthetic natural gas: From coal, dry biomass, and power-to-gas applications. *Focus Catal.* **2016**, *2016*, 7. [CrossRef]
40. Cheng, C.; Shen, D.; Xiao, R.; Wu, C. Methanation of syngas (H 2 /CO) over the different Ni-based catalysts. *Fuel* **2017**, *189*, 419–427. [CrossRef]
41. Charisiou, N.; Siakavelas, G.; Papageridis, K.; Baklavaridis, A.; Tzounis, L.; Polychronopoulou, K.; Goula, M. Hydrogen production via the glycerol steam reforming reaction over nickel supported on alumina and lanthana-alumina catalysts. *Int. J. Hydrog. Energy* **2017**, *42*, 13039–13060. [CrossRef]
42. Melchor-Hernández, C.; Gómez-Cortés, A.; Diaz, G. Hydrogen production by steam reforming of ethanol over nickel supported on La-modified alumina catalysts prepared by sol–gel. *Fuel* **2013**, *107*, 828–835. [CrossRef]
43. Sing, K.S.; Williams, R.T. Physisorption hysteresis loops and the characterization of nanoporous materials. *Adsorpt. Sci. Technol.* **2004**, *22*, 773–782. [CrossRef]
44. Bang, Y.; Han, S.J.; Gil Seo, J.; Youn, M.H.; Song, J.H.; Song, I.K. Hydrogen production by steam reforming of liquefied natural gas (LNG) over ordered mesoporous nickel–alumina catalyst. *Int. J. Hydrog. Energy* **2012**, *37*, 17967–17977. [CrossRef]

45. Mo, W.; Ma, F.; Ma, Y.; Fan, X. The optimization of Ni–Al_2O_3 catalyst with the addition of La2O3 for CO_2–CH4 reforming to produce syngas. *Int. J. Hydrog. Energy* **2019**, *44*, 24510–24524. [CrossRef]
46. Bizkarra, K.; Barrio, V.; Yartu, A.; Requies, J.; Arias, P.L.; Cambra, J.F. Hydrogen production from n-butanol over alumina and modified alumina nickel catalysts. *Int. J. Hydrog. Energy* **2015**, *40*, 5272–5280. [CrossRef]
47. García-Lario, A.L.; Aznar, M.; Martinez, I.; Grasa, G.S.; Murillo, R. Experimental study of the application of a NiO/NiAl 2 O 4 catalyst and a CaO-based synthetic sorbent on the Sorption Enhanced Reforming process. *Int. J. Hydrog. Energy* **2015**, *40*, 219–232. [CrossRef]
48. Lee, J.-H.; Lee, E.-G.; Joo, O.-S.; Jung, K.-D. Stabilization of Ni/Al_2O_3 catalyst by Cu addition for CO_2 reforming of methane. *Appl. Catal. A Gen.* **2004**, *269*, 1–6. [CrossRef]
49. Hossain, Z.; Chowdhury, M.B.; Charpentier, P.A. Effect of surface acidity of Al_2O_3 supported metal catalysts on catalytic activity and carbon deposition during SCWG of glucose. *Biomass Bioenergy* **2019**, *124*, 142–150. [CrossRef]
50. Quindimil, A.; De-La-Torre, U.; Pereda-Ayo, B.; Davó-Quiñonero, A.; Bailón-García, E.; Lozano-Castelló, D.; González-Marcos, J.A.; Bueno-López, A.; González-Velasco, J.R. Effect of metal loading on the CO_2 methanation: A comparison between alumina supported Ni and Ru catalysts. *Catal. Today* **2020**, *356*, 419–432. [CrossRef]
51. Song, K.H.; Yan, X.; Koh, D.J.; Kim, T.; Chung, J.-S. La effect on the long-term durability of Ni-Mg-Al 2 O 3 catalysts for syngas methanation. *Appl. Catal. A Gen.* **2017**, *530*, 184–192. [CrossRef]
52. Charisiou, N.; Iordanidis, A.; Polychronopoulou, K.; Yentekakis, I.; Goula, M. Studying the stability of Ni supported on modified with CeO2 alumina catalysts for the biogas dry reforming reaction. *Mater. Today Proc.* **2018**, *5*, 27607–27616. [CrossRef]
53. Zhang, Z.; Wang, Y.; Sun, K.; Shao, Y.; Zhang, L.; Zhang, S.; Zhang, X.; Liu, Q.; Chen, Z.; Hu, X. Steam reforming of acetic acid over Ni–Ba/Al_2O_3 catalysts: Impacts of barium addition on coking behaviors and formation of reaction intermediates. *J. Energy Chem.* **2020**, *43*, 208–219. [CrossRef]
54. Sengupta, S.; Deo, G. Modifying alumina with CaO or MgO in supported Ni and Ni–Co catalysts and its effect on dry reforming of CH4. *J. CO_2 Util.* **2015**, *10*, 67–77. [CrossRef]
55. Tan, M.; Wang, X.; Shang, X.; Zou, X.; Lu, X.; Ding, W. Template-free synthesis of mesoporous γ-alumina-supported Ni–Mg oxides and their catalytic properties for prereforming liquefied petroleum gas. *J. Catal.* **2014**, *314*, 117–131. [CrossRef]
56. Requies, J.; Cabrero, M.; Barrio, V.; Güemez, M.; Cambra, J.; Arias, P.; Pérez-Alonso, F.; Ojeda, M.; Peña, M.; Fierro, J. Partial oxidation of methane to syngas over Ni/MgO and Ni/La2O3 catalysts. *Appl. Catal. A Gen.* **2005**, *289*, 214–223. [CrossRef]
57. Yashnik, S.A.; Kuznetsov, V.V.; Ismagilov, Z.R. Effect of χ-alumina addition on H 2 S oxidation properties of pure and modified γ-alumina. *Chin. J. Catal.* **2018**, *39*, 258–274. [CrossRef]
58. Zamani, M.; Delfani, A.M.; Jabbari, M. Scavenging performance and antioxidant activity of γ-alumina nanoparticles towards DPPH free radical: Spectroscopic and DFT-D studies. *Spectrochim. Acta Part A Mol. Biomol. Spectrosc.* **2018**, *201*, 288–299. [CrossRef] [PubMed]
59. Wulfsberg, G. *Inorganic Chemistry*; University Science Books: Mill Valley, CA, USA, 2000.
60. Italiano, C.; Llorca, J.; Pino, L.; Ferraro, M.; Antonucci, V.; Vita, A. CO and CO_2 methanation over Ni catalysts supported on CeO2, Al_2O_3 and Y2O3 oxides. *Appl. Catal. B Environ.* **2020**, *264*, 118494. [CrossRef]
61. Liu, K.; Xu, X.; Xu, J.; Fang, X.; Liu, L.; Wang, X. The distributions of alkaline earth metal oxides and their promotional effects on Ni/CeO2 for CO_2 methanation. *J. CO_2 Util.* **2020**, *38*, 113–124. [CrossRef]
62. NIST XPS Database. Selected Element Search Result. Available online: https://srdata.nist.gov/xps/EngElmSrchQuery.aspx?EType=PE&CSOpt=Retri_ex_dat&Elm=Ni (accessed on 12 July 2019).
63. Paglia, G. Determination of the Structure of Y-Alumina Using Empirical and First Principle Calculations Combined with Supporting Experiments. Ph.D. Thesis, Curtin University of Technology, Perth, Australia, February 2004.
64. Segal, F.M.; Corrêa, M.F.; Bacani, R.; Castanheira, B.; Politi, M.J.; Brochsztain, S.; Triboni, E.R. A Novel Synthesis Route of Mesoporous γ-Alumina from Polyoxohydroxide Aluminum. *Mater. Res.* **2018**, *21*. [CrossRef]
65. Shen, X.; Garces, L.-J.; Ding, Y.; Laubernds, K.; Zerger, R.P.; Aindow, M.; Neth, E.J.; Suib, S.L. Behavior of H2 chemisorption on Ru/TiO2 surface and its application in evaluation of Ru particle sizes compared with TEM and XRD analyses. *Appl. Catal. A Gen.* **2008**, *335*, 187–195. [CrossRef]
66. Chen, G.; Wang, R.; Zhao, W.; Kang, B.; Gao, D.; Li, C.; Lee, J.Y. Effect of Ru crystal phase on the catalytic activity of hydrolytic dehydrogenation of ammonia borane. *J. Power Sources* **2018**, *396*, 148–154. [CrossRef]
67. Rah, I.J.; Kim, T.W.; Kim, J.; Lee, D.; Park, E.D. Selective CO oxidation in the hydrogen stream over Ru/Al@Al_2O_3 catalysts. *Catal. Today* **2020**, *352*, 148–156. [CrossRef]
68. Lesbani, A.; Sitompul, S.O.C.; Mohadi, R.; Hidayati, N. Characterization and utilization of calcium oxide (CaO) thermally decomposed from fish bones as a catalyst in the production of biodiesel from waste cooking oil. *Makara J. Technol.* **2016**, *20*, 121. [CrossRef]
69. Wang, Y.-Z.; Zhong, D.-L.; Duan, H.-L.; Song, C.-M.; Han, X.-T.; Ma, X.-R. Removal of naphthenic acids from crude oils by catalytic decomposition using Mg–Al hydrotalcite/γ-Al_2O_3 as a catalyst. *Fuel* **2014**, *134*, 499–504. [CrossRef]
70. Malinowski, J.; Dercz, G.; Prusik, K.; Pajak, L.; Pielaszek, R.; Pudlo, W. Structure studies on nanocrystalline powder of MgO xerogel prepared by sol-gel method. *Mater. Sci. Pol.* **2009**, *27*, 201–207.
71. Selvarajan, K.E.P.; Balasubramanian, K. Preparation and studies of cerium dioxide (CeO2) nanoparticles by microwave-assisted solution method. *Recent Res. Sci. Technol.* **2010**, *2*, 37–41.

72. Seki, H.; Saito, H.; Toko, K.; Hosono, Y.; Higo, T.; Gil Seo, J.; Maeda, S.; Hashimoto, K.; Ogo, S.; Sekine, Y. Effect of Ba addition to Ga-α-Al_2O_3 catalyst on structure and catalytic selectivity for dehydrogenation of ethane. *Appl. Catal. A Gen.* **2019**, *581*, 23–30. [CrossRef]
73. Saravani, H.; Khajehali, M. Synthesis and characterization of lanthanum oxide and lanthanumoxid carbonate nanoparticles from thermalizes of [La(acacen)(NO3)(H2O) complex. *Orient. J. Chem.* **2016**, *32*, 491–498. [CrossRef]
74. Claude, V.; Mahy, J.G.; Douven, S.; Lohay, T.; Micheli, F.; Lambert, S.D. Sol-gel Ni-based/γ-Al_2O_3 as efficient catalysts for toluene reforming: Catalytic activity during long-term experiments and in presence of H2S. *J. Environ. Chem. Eng.* **2020**, *8*, 104528. [CrossRef]
75. Liu, Q.; Wang, S.; Zhao, G.; Yang, H.; Yuan, M.; An, X.; Zhou, H.; Qiao, Y.; Tian, Y. CO_2 methanation over ordered mesoporous NiRu-doped CaO-Al_2O_3 nanocomposites with enhanced catalytic performance. *Int. J. Hydrog. Energy* **2018**, *43*, 239–250. [CrossRef]